EUROPEAN RESPIRATORY journal

FLAGSHIP SCIENTIFIC JOURNAL OF ERS

Early View

Original article

TNF-mediated alveolar macrophage necroptosis drives disease pathogenesis during Respiratory Syncytial Virus infection

Leonardo Duarte Santos, Krist Helen Antunes, Stéfanie Primon Muraro, Gabriela Fabiano de Souza, Amanda Gonzalez da Silva, Jaqueline de Souza Felipe, Larissa Cardoso Zanetti, Rafael Sanguinetti Czepielewski, Karen Magnus, Marcelo Scotta, Rita Mattiello, Fabio Maito, Ana Paula Duarte de Souza, Ricardo Weinlich, Marco Aurélio Ramirez Vinolo, Bárbara Nery Porto

Please cite this article as: Santos LD, Antunes KH, Muraro Séfanie P, *et al*. TNF-mediated alveolar macrophage necroptosis drives disease pathogenesis during Respiratory Syncytial Virus infection. *Eur Respir J* 2020; in press (https://doi.org/10.1183/13993003.03764-2020).

TNF-mediated alveolar macrophage necroptosis drives disease pathogenesis during Respiratory Syncytial Virus infection

Leonardo Duarte Santos[1], Krist Helen Antunes[1], Stéfanie Primon Muraro[1,6*], Gabriela Fabiano de Souza[1,6*], Amanda Gonzalez da Silva[1], Jaqueline de Souza Felipe[2], Larissa Cardoso Zanetti[3], Rafael Sanguinetti Czepielewski[1,7], Karen Magnus[1], Marcelo Scotta[4], Rita Mattiello[4], Fabio Maito[5], Ana Paula Duarte de Souza[1], Ricardo Weinlich[3], Marco Aurélio Ramirez Vinolo[2], Bárbara Nery Porto[1,8,#]

1 Laboratory of Clinical and Experimental Immunology, Infant Center, School of Life and Health Science, Pontifical Catholic University of Rio Grande do Sul, Porto Alegre, RS, Brazil.

2 Laboratory of Immunoinflammation, Department of Genetics, Evolution, Microbiology and Immunology, Institute of Biology, University of Campinas, Campinas, SP, Brazil.

3 Hospital Israelita Albert Einstein, São Paulo, SP, Brazil.

4 Infant Center, School of Life and Health Science, Pontifical Catholic University of Rio Grande do Sul, Porto Alegre, RS, Brazil.

5 Laboratory of Oral Pathology, Health Science School, Pontifical Catholic University of Rio Grande do Sul, Porto Alegre, RS, Brazil.

6 Present address: Laboratory of Emerging Viruses, Department of Genetics, Evolution, Microbiology and Immunology, Institute of Biology, University of Campinas, Campinas, SP, Brazil.

7 Present address: Department of Pathology and Immunology, Washington University School of Medicine, St. Louis, MO, USA.

8 Present address: Program in Translational Medicine, The Hospital for Sick Children, Toronto, ON, Canada.

*These authors contributed equally to this work.

[#]**To whom correspondence should be addressed:** Bárbara N. Porto (barbara.porto@sickkids.ca; bnporto@hotmail.com)

ORCID ID: https://orcid.org/0000-0002-1995-9874

Keywords: Respiratory Syncytial Virus; Alveolar Macrophage; Necroptosis; TNF; Bronchiolitis.

Author contributions

BNP conceived the study. BNP and MARV designed and supervised the experiments. BNP and LDS wrote the manuscript with input from MARV, RW and APDS. LDS, KHA, SPM, GFS, AGS, JFS, LCZ, RSC and KM performed the experiments and analyzed the data. FM performed the lung histopathological and immunohistochemistry analysis. MS, RM and APDS provided the patients' nasal washes and contributed to the data analysis. All authors reviewed and commented on the manuscript.

Abstract

Respiratory Syncytial Virus (RSV) is the major cause of acute bronchiolitis in infants under 2 years old. Necroptosis has been implicated in the outcomes of respiratory virus infections. Here we report that RSV infection triggers necroptosis in primary mouse macrophages and human monocytes in a RIPK1-, RIPK3-, and MLKL-dependent manner. Moreover, necroptosis pathways are harmful to RSV clearance from alveolar macrophages. Additionally, *Ripk3-/-* mice were protected from RSV-induced weight loss and presented reduced viral loads in the lungs.

Alveolar macrophage depletion also protected mice from weight loss and decreased lung RSV virus load. Importantly, alveolar macrophage depletion abolished the upregulation of *Ripk3* and *Mlkl* gene expression induced by RSV infection in the lung tissue.

Autocrine TNF mediated RSV-triggered macrophage necroptosis and necroptosis pathways were also involved in TNF secretion even when macrophages were committed to cell death, which can worsen lung injury during RSV infection. In line, *Tnfr1-/-* mice had a marked decrease in *Ripk3* and *Mlkl* gene expression and a sharp reduction in the numbers of necrotic alveolar macrophages in the lungs. Finally, we provide evidence that elevated nasal levels of TNF are associated with disease severity in infants with RSV bronchiolitis.

We propose that targeting TNF and/or the necroptotic machinery may be valuable as therapeutic approaches to reduce the respiratory morbidity caused by RSV infection in young children.

Take-home message

RIPK1-, RIPK3-, and MLKL-dependent alveolar macrophage necroptosis triggered by RSV infection is mediated by autocrine TNF and harmful to viral clearance. This study suggests that alveolar macrophage necroptosis drives RSV disease pathogenesis.

Introduction

Respiratory Syncytial Virus (RSV) is the most frequent cause of hospitalization due to acute bronchiolitis and viral pneumonia in infants under 2 years of age [1, 2] and has been estimated to be responsible for up to 200,000 deaths every year worldwide [2, 3]. Infants born preterm or with high-risk medical conditions, such as congenital heart disease or chronic lung disease, have an increased risk of developing a severe RSV disease [4]. Furthermore, accumulating evidence suggests that RSV infection in childhood may predispose to recurrent wheezing and asthma later in life [5, 6]. Although the World Health Organization has designated RSV as a high-priority target for vaccine development, so far there is no clinically approved RSV vaccine. Therefore, the understanding of how RSV interacts with the host is of the utmost importance to better characterize the disease pathogenesis and to develop new therapies.

Alveolar macrophages (AM) account for nearly 95% of leukocytes in the airways and are the first immune cells to encounter pulmonary pathogens [7, 8]. For this reason, their response to infection can critically influence the outcomes of infectious diseases [7, 9]. In this scenario, emerging evidence has revealed that AM death also plays an important role in determining the pathogenesis of pulmonary viral infections [10, 11].

Necroptosis is considered a pro-inflammatory form of cell death that leads to the release of intracellular contents, which may act as damage-associated molecular patterns (DAMPs), stimulating immune cells [12]. Necroptosis is driven by the assembly of a multiprotein complex consisting of Receptor Interacting Protein Kinase 1 (RIPK1) and RIPK3, leading to the activation of the pseudokinase Mixed-Lineage Kinase Domain-Like (MLKL) [13, 14]. Necroptotic cell death is effective in restraining the spread of intracellular pathogens, such as viruses, by eliminating replication sites [15, 16]; however, it imposes a cost on the host by exacerbating inflammation and tissue injury following infection. Accordingly, it has been previously shown that Influenza A H1N1 virus induces necroptosis in alveolar epithelial cells and that necroptosis is a pathological feature of the infection, being responsible for the high morbidity and mortality of infected animals [17]. Furthermore, the lack of RIPK3 causes decreased cytokine expression and alleviates Influenza A H7N9 virus-induced acute lung injury in mice [18]. It has been recently reported that RSV triggers alveolar epithelial cells and THP-1 cell necroptosis [19, 20]. Nevertheless, whether RSV induces alveolar macrophage necroptosis and whether its effect is protective or detrimental to the host are yet to be demonstrated.

Here we report that an active RSV infection is necessary and sufficient to trigger necroptosis in primary mouse macrophages and human monocytes in a RIPK1-, RIPK3-, and MLKL-dependent manner. Moreover, the activation of necroptosis pathways is detrimental to viral clearance. *Ripk3-/-* mice were protected from RSV-induced weight loss and presented reduced viral loads in the lungs. Surprisingly, AM have shown to play a harmful role during RSV infection and AM depletion abolished the upregulation of RIPK3 and MLKL mRNA levels in the lung tissue induced by RSV infection. Moreover, autocrine TNF mediates RSV-triggered macrophage necroptosis and *Tnfr1-/-* mice had a marked decrease in the expression of RIPK3 and MLKL mRNA and a sharp reduction in the numbers of dead AM in the lungs. These data suggest that TNF-mediated alveolar macrophage necroptosis plays a significant role in the pathogenesis of RSV infection.

Methods

Virus preparation.

The virus production of RSV A2 strain (kindly donated by Dr. Fernando Polack, Fundación Infant, Argentina) was obtained in VERO cells (ATCC CCL-81) cultured in Opti-MEM medium (Gibco by Life Technologies™, Grand Island, NY, USA) with 2% FBS (Gibco by Life Technologies™, Grand Island, NY, USA) at 37°C under 5% CO_2. To assess viral titer, VERO cells were infected with RSV in medium without serum followed by a carboxymethylcellulose plaque assay. Lysis plate titration was performed using an anti-RSV F protein antibody (Millipore, Billerica, MA, USA) and viral titer was expressed as plaque forming units (PFU). The virus aliquots were stored at -80°C.

RSV clinical isolates preparation.

Nasopharyngeal aspirates from 2 patients were diluted in DMEM low glucose (Gibco by Life Technologies™, Grand Island, NY, USA) (5 mL) containing 1000 µg/mL of gentamycin and inoculated into VERO cells culture. After 1 h incubation at 37°C for complete viral adsorption, the viral inoculum was removed and 10 mL of Opti-MEM supplemented with 2% of FBS and 1000 µg/mL of gentamycin were added into the flask. The culture was incubated at 37°C with 5% CO_2 until the cytopathic effect was visualized. Then, cells were harvested, centrifuged and the cell pellet was subjected to snap freeze-thaw cycles to obtain new viral particles. Afterwards, sucrose cryoprotector was added to the viral aliquots and stored in -80°C until titration or further analysis. Lysis plate titration was performed using an anti-RSV antibody and viral titer was expressed as plaque forming units (PFU). The viral nomenclature was made based on the city of isolation/strain number/year (RSV POA10/2018 and RSV POA43/2018). Clinical isolates were assayed by real-time PCR and were identified as follows: RSV POA10/2018 is RSV subtype B and RSV POA43/2018 is RSV subtype A.

Mouse macrophages isolation and stimulation.

Alveolar macrophages.

Alveolar macrophages were collected by bronchoalveolar lavage through flushing the lungs three times with 1 mL of chilled PBS supplemented with EDTA (5 mM). The lavage was repeated twice and alveolar macrophages from several mice were pooled. Cells were seeded at 3 x 10^5/well in AIM-V medium (Gibco by Life Technologies™, Grand Island, NY, USA) overnight. Afterwards, non-adherent cells were removed by washing, and adherent cells were stimulated with different multiplicity of infections (MOIs) of RSV (0.1 – 10) for 2, 4 or 6 h at 37°C under 5% CO_2. Then, macrophages were labeled with Fixable Viability Dye eFluor® 780 (eBioscience by Thermo Fisher Scientific, Waltham,

MA, USA), harvested by gentle scraping and the percent of dead cells was analyzed by flow cytometry, as described below.

Peritoneal macrophages.

Peritoneal macrophages were obtained 3 days after intraperitoneal instillation of 3 mL of 3% thioglycollate by peritoneal washing with chilled PBS. Cells were seeded at 3 x 10^5/well in AIM-V medium overnight. Afterwards, non-adherent cells were removed by washing, and adherent cells were stimulated with different MOIs of RSV (0.1 – 10) for 2, 4 or 6 h at 37^{o}C under 5% CO_2. After that, macrophages were labeled with Fixable Viability Dye eFluor® 780, harvested and the percent of dead cells was analyzed by flow cytometry.

Human monocytes isolation and stimulation.

Peripheral blood mononuclear cells (PBMCs) were isolated from healthy volunteer donors (with a mean age of 29 years, from both sexes) after signing an informed consent form. Twenty milliliters of whole blood were collected and subjected to a Histopaque-1077 (Sigma-Aldrich, Saint Louis, MO, USA) gradient centrifugation for 30 minutes. PBMCs were seeded at 3 x 10^5/well in RPMI 1640 medium (Gibco by Life Technologies™, Grand Island, NY, USA) containing 10% FBS overnight. Afterwards, non-adherent cells were removed by washing, and adherent cells were infected with RSV at an MOI of 1 for 6 h at 37^{o}C. After that, cells were labeled with Fixable Viability Dye eFluor® 780, harvested and the percent of dead cells was analyzed by flow cytometry.

Cell lines.

Human monocyte-like cell line (THP-1, ATCC TIB-202) and promonocytic cell line (U937, ATCC CRL-1593.2) were cultured in RPMI 1640 medium supplemented with 10% FBS. For differentiation to macrophage-like cells, U937 cells were seeded at a density of 2x10^5/cm^2 in RPMI 1640 with 10% FBS containing PMA (50 ng/mL) for 24 h [21]. Human adenocarcinoma alveolar epithelial cell line (A549, ATCC CCL-185) was cultured in DMEM low glucose supplemented with 10% FBS. All cell lines were tested for mycoplasma contamination. THP-1 cells and U937 cells differentiated to macrophage-like cells were infected with RSV at an MOI of 1 for 6 h at 37^{o}C. Afterwards, cells were labeled with Fixable Viability Dye eFluor® 780 and the percent of dead cells was analyzed by flow cytometry.

TNF measurements.

The concentrations of TNF in mouse macrophage supernatants and in the supernatants of human monocytes and nasal washes obtained from RSV+ and RSV- infants were determined using ELISA (Sigma-Aldrich, Saint Louis, MO, USA), following the manufacturer's instructions.

LDH release measurements.

LDH release was detected in macrophage or monocyte supernatants using the CytoTox 96 Non-Radioactive Cytotoxicity Assay kit from Promega (Madison, Wisconsin, EUA), according to the manufacturer's instructions. Readings were carried out at 490 nm wavelength, using EZ Read 400 microplate reader from Biochrom (Holliston, MA, USA) and expressed as % LDH release.

RIPK3, MLKL and CXCL1 detection by real-time PCR.

Mouse lungs or alveolar macrophages (3 x 10^5/well) were suspended in Brazol reagent (LGC Biotecnologia, Cotia, SP, BR) (1 mL) and the protocol for total RNA extraction was carried out according to the manufacturer's instructions. RNA was reverse-transcribed into cDNA using a High Capacity cDNA Reverse Transcription Kit (Applied Biosystems by Thermo Fisher Scientific, Waltham, MA, USA) and fluorometric quantification was performed with Qubit (ThermoFisher Scientific, Waltham, MA, USA). The expression of the *Ripk3*, *Mlkl* and *Cxcl1* genes was performed using specific primers and probes TaqMan Assay (Mm00444947_m1; Mm01244222_m1; Mm04207460_m1, respectively) using the *β-actin* gene (Mm02619580_g1) as an endogenous control. Quantification of gene expression was carried out using StepOne (Applied Biosystems by ThermoFisher Scientific, Waltham, MA, USA). A total of 15 ng of cDNA was used for each reaction. The target gene expression was determined using the $2^{-\Delta Ct}$ method (fold change over control expression). The delta value was calculated by subtracting the CT value for *β-actin* from the CT value for *Ripk3*, *Mlkl* and *Cxcl1* for each sample.

MLKL detection by western blotting.

Alveolar macrophages (3 x 10^5/well) were infected with RSV (MOI 1) for the indicated times. Afterwards, cells were harvested and lysed in RIPA buffer containing a protease inhibitor cocktail. Cell lysates were boiled and subjected to electrophoresis in SDS-polyacrylamide gel (10%) in reducing conditions. The quantified proteins were transferred to a methanol-activated PVDF membrane at 4^{o}C for 2 h. Then, the membranes were blocked with non-fat milk-TBS-T solution for 1 h at room temperature and incubated overnight with anti-MLKL (1:1000, cat# AP14272, Abgent) antibodies followed by HRP anti-rabbit secondary antibody (1:5000, cat#31460, ThermoFisher Scientific). As an endogenous control, anti-GAPDH antibody (1:5000, cat# MA5-15738, ThermoFisher Scientific), followed by HRP anti-mouse secondary antibody (1:5000, cat# 31430, ThermoFisher

Scientific) was used. The detection of MLKL expression was performed using the ECL system (Amersham ECL Prime Western Blotting Detection reagent, GE) and the membrane was imaged using ChemiDoc Imaging System (BioRad). The densitometry analysis was performed using ImageJ 1.43 software (NIH). MLKL bands were normalized to GAPDH bands.

Animals and RSV infection.

For *ex vivo* experiments, female Balb/c mice with 8-10 weeks of age were supplied by the breeding facilities of Centro de Modelos Biológicos Experimentais (CeMBE/PUCRS). Animal procedures were reviewed and approved by the Ethics Committee on Animal Use of PUCRS (CEUA/PUCRS) under protocol number 8049. For *in vivo* experiments, female TNF-α receptor p55 [p55TNF-knock-out (KO) or TNFR1-/-] and C57/BL6 WT mice at age 8-10 weeks were supplied by the breeding facilities of Centro de Criação de Camundongos Especiais da Faculdade de Medicina de Ribeirão Preto (FMRP/USP), whereas female RIPK3-/- and C57/BL6 WT mice at age 8-10 weeks were supplied by Dr. Vishva Dixit (Genentech, Inc., South San Francisco, California, USA) [22] and housed in the breeding facilities of Centro de Criação de Camundongos Especiais da Faculdade de Medicina de Ribeirão Preto (FMRP/USP). All mice were kept in regular filter-top cages with free access to sterile water and food. Animal procedures were reviewed and approved by the Ethics Committee on Animal Use of the Institute of Biology (protocol numbers 4740-1/2017 and 4740-1(A)/2018) and performed according to the Declaration of Helsinki conventions for the use and care of animals.

For RSV infection, mice were anesthetized with 5% isoflurane and infected intranasally with RSV A2 strain (10^7 PFU/animal). All animals were weighed daily. Data analysis was performed 5 days post infection. Bronchoalveolar lavage (BAL) fluid was collected and left lungs were removed after perfusion with formalin for histopathological and immunohistochemistry analysis.

BAL fluid collection.

Mice were anesthetized with intraperitoneal administration of ketamine (0.4 mg/g)/xylazine (0.2 mg/g) solution and the tracheas were cannulated. The lungs were washed twice with 1 mL of chilled RPMI 1640 medium. BAL was centrifuged, the supernatants collected for cytokine analysis and the pellets suspended for total and differential cell count and flow cytometry. For differential cell counting, the cytospin slides were stained with H&E and the counting procedure was performed by an experienced investigator in a blinded manner.

Histopathological and immunohistochemistry analysis.

For the histopathological analysis, the left lungs were embedded in paraffin blocks, cut into 4-μm sections and stained with H&E. The peribronchial and perivascular inflammation was scored according to Barends et al [23], as absent (0), minimal (1), slight (2), moderate (3), marked (4) or severe (5). Slide analysis was performed in a blinded manner. For immunohistochemistry, the lung sections were submitted to antigen recovery and subsequent labeling with anti-RSV F protein antibody.

Alveolar macrophage depletion.

Alveolar macrophages were depleted by an intranasal administration of clodronate-liposomes (Sigma-Aldrich, Saint Louis, MO, USA) (500μg/animal) or PBS-liposomes, as a control. Mice were infected with RSV (10^7 PFU/animal) 24 hours later. The animals were weighed daily and data analysis was performed 5 days post infection, as described above. Macrophage depletion was confirmed by flow cytometry analysis in BAL samples.

Flow cytometry.

To analyze the percent of cell death following RSV infection *in vitro*, cells were labeled with Fixable Viability Dye eFluor® 780 (1:1000) for 30 minutes on ice protected from light and then harvested with gentle scraping. After that, the cells were washed with PBS and cytometry buffer was added. Samples were acquired using BD FACS Verse (BD Biosciences, San Jose, CA, USA) flow cytometer and analyzed using FlowJo software (version 10, Tree Star Inc., San Jose, CA, USA).

Cells isolated from BAL of infected mice were incubated with Mouse Fc Block for 20 minutes and then labeled with Fixable Viability Dye eFluor® 780 (1:1000) for 30 minutes on ice. Afterwards, cells were stained with surface antibodies anti-CD11c (1:200, clone N418, BioLegend, San Diego, CA, USA), anti-F4/80 (1:200, clone BM8, BioLegend, San Diego, CA, USA) and anti-CD170 (Siglec-F) (1:200, clone 1RNM44N, (eBioscience by Thermo Fisher Scientific, Waltham, MA, USA).) for 30 minutes on ice. Samples were acquired using BD FACS Verse flow cytometer and analyzed using FlowJo software.

Viral load quantitation by real-time PCR.

Total lung RNA was extracted and cDNA was synthesized using GoScript reverse transcriptase kit (Promega, Madison, WI, USA), following manufacturer's instructions. The amplification of RSV F protein gene was performed using the indicated specific primers and probes: forward primer - 5'-AACAGATGTAAGCAGCTCCGTTATC-3', reverse primer - 5'-GATTTTTATTGGATGCTGTACATTT-3' and probe - 5' FAM/TGCCATAGCATGACACAATGGCTCCT-TAMRA/-3' by real-time PCR. Primer sequences

were synthesized and cloned into pUC57 plasmids (GenScript, Piscataway, NJ, USA) to perform a 10-fold dilution and generate a standard curve for calculation of the viral load. The values obtained from viral copies (based on concentration of the plasmid control) were calculated relative to the weight of the pre-weighed lung portion (copies/g of lung).

Human samples.

We obtained nasopharyngeal lavage samples from infants hospitalized with bronchiolitis in the first year of life from 2016 to 2018. The samples were from patients who had up to 72 h of clinical signs of a lower respiratory tract infection, such as cough, wheezing and/or respiratory distress. All patients underwent data collection and nasopharyngeal wash for the identification of respiratory viruses on the first day of hospitalization. The presence of RSV in patients' samples was identified by both immunofluorescence and RT-PCR. After collection, nasopharyngeal wash samples were diluted in 1 mL saline, homogenized and centrifuged. The supernatant was collected and frozen at -80^{o}C until further analysis.

Ethics statement.

For infant sample collection, the parents or legal guardians of all participants signed an informed consent form before sample collection. The study was reviewed and approved by the Research Ethics Committee of PUCRS (CEP/PUCRS) under protocol numbers 1.158.826 and

2.471.678. All procedures followed the standards established by the Declaration of Helsinki.

Statistical analysis.

Data were presented as mean ± SEM. All *in vitro* experiments were performed in triplicates and repeated at least two times. *In vivo* experiments were performed two times ($n \geq 3$ mice per group in each experiment). The results obtained were analyzed using GraphPad Prism 6 statistical software package. Comparisons between multiple groups were analyzed with one-way ANOVA and a posteriori Tukey or Bonferroni test. When appropriate, unpaired Student's *t* test or Mann Whitney test were employed. The level of significance was set at $p \leq 0.05$.

Results

RSV induces necrosis in primary mouse macrophages, human monocytes and macrophage-like cell lines.

To evaluate the effect of RSV on alveolar macrophage necrosis, cells were infected with RSV (MOI 1) for 6 h and cell death was assessed by a viability dye that permeates the damaged membrane of dead cells. Our results show that RSV triggered alveolar macrophage necrosis (Fig. 1A), and that the effect of RSV on macrophage death is dependent on virus replication, since UV inactivation impaired RSV-induced death (Fig. 1A). To confirm that alveolar macrophages can be infected by RSV, we quantified the viral load after 6 h of infection. Indeed, RSV was able to infect mouse alveolar macrophages (Fig. 1B). Interestingly, RSV was also able to kill peritoneal macrophages (Fig. 1C) and again, UV-inactivated RSV failed to trigger cell death (Fig. 1C), indicating that an active RSV infection is necessary to promote macrophage death. Further characterization of RSV-induced necrosis revealed that both alveolar and peritoneal macrophage necrosis occurs in a concentration-dependent manner (Supplementary Fig. 1A, D). Similar results were observed when LDH release was quantified after infection (Supplementary Fig. 1B, E). Cell death could be detected as early as 2 h post-infection in alveolar macrophages (Supplementary Fig. 1C) and 4 h post-infection in peritoneal macrophages (Supplementary Fig. 1F). Moreover, we found that RSV was able to induce necrosis in human monocytes (Supplementary Fig. 2A, D), in the human macrophage-like THP-1 cells (Supplementary Fig. 2B, E) and in the human U937 monocytic cells differentiated to macrophage-like cells with PMA (Supplementary Fig. 2C, F). We confirmed that RSV infects and replicates in all these cell types (Supplementary Fig. 2G), and used the human lung epithelial cell line A549 cells as a positive control for RSV replication (Supplementary Fig. 2G). Finally, we tested the effect of RSV clinical isolates on human monocyte necrosis. Two different RSV clinical isolates were able to promote human monocyte necrosis (Fig. 1D). Altogether, these data indicate that alveolar and peritoneal mouse macrophages, human monocytes and human macrophage-like cell lines are susceptible to RSV infection-induced necrosis. Furthermore, our results show that clinical RSV strains isolated from patients also trigger necrosis in human monocytes.

RIPK1, RIPK3 and MLKL are required for RSV-induced macrophage necroptosis.

Most studies on necroptosis commonly stimulate immune and non-immune cells with inflammatory agents in the absence of caspase signaling (using benzyloxycarbonyl-Val-Ala-Asp-fluoromethyl ketone, zVAD-FMK) [24]. Our results demonstrate that the treatment of macrophages with zVAD-

FMK prior to RSV infection did not reduce cell death compared to RSV alone (Fig. 2A), suggesting that RSV infection does not induce apoptosis and does not require caspase inhibition by zVAD-FMK to induce necrosis in macrophages. To determine the role of RIPK1 on RSV-driven macrophage death, cells were pretreated with NEC-1, which targets the kinase activity of RIPK1 [25]. Pre-treating macrophages with NEC-1 significantly impaired cell death induced by RSV (Fig. 2B). The role of RIPK3 on RSV-triggered macrophage death was examined by infecting macrophages from *Ripk3-/-* mice and littermate control WT mice with RSV for 6 h. Remarkably, *Ripk3-/-* macrophages were completely resistant to RSV-induced cell death at this timepoint (Fig. 2C). Likewise, pharmacological suppression of RIPK3 by GW42X [26] protected human monocytes from death promoted by RSV infection (Fig. 2D) and necrosulfonamide (NSA) inhibition of MLKL [14] blocked RSV-triggered human monocyte necroptosis (Fig. 2E). We next sought to investigate whether the inhibition of necroptosis pathways would impact RSV replication. Indeed, the pharmacological blockade of RIPK1, RIPK3 and MLKL significantly reduced RSV viral loads in human monocytes (Fig. 2F). Similarly, *Ripk3-/-* macrophages exhibited a significantly lower viral load when compared to WT macrophages infected with RSV (Fig. 2G). Interestingly, caspases inhibition by zVAD-FMK did not affect viral load in human monocytes (Fig. 2F), suggesting that caspases are not involved in virus replication during RSV infection. Then, we decided to verify whether RSV would induce RIPK3 and MLKL expression in macrophages. RSV infection of macrophages resulted in significant RIPK3 and MLKL mRNA expression 6 h after infection (Fig. 2H, I) and an increase in MLKL protein levels at 2 h and 4 h post-infection (Supplementary Fig. 3). Taken together, these results indicate that RSV sufficiently promotes mouse macrophage and human monocyte necroptosis through the activation of RIPK1, RIPK3 and MLKL and that necroptosis pathways are detrimental to viral clearance.

RIPK3 exacerbates lung pathology during RSV infection partially dependent on cell death.

It has been previously demonstrated that genetic deletion of RIPK3 protected cIAP2-deficient mice from morbidity and mortality induced by Influenza A H1N1 virus infection [17]. Furthermore, *Ripk3-/-* mice have shown higher survival rates and less weight loss and inflammatory cell infiltration compared to WT mice when infected with Influenza H7N9 virus [18]. Based on the literature and on our findings showing that RSV induces macrophage necroptosis through RIPK3 activation, we sought to investigate the role of RIPK3 during RSV infection *in vivo*. Notably, *Ripk3-/-* mice were protected from RSV-induced weight loss compared to WT mice (Fig. 3A) and this was associated with a marked

reduction in viral loads in the lung (Fig. 3B). Moreover, *Ripk3-/-* mice presented a significant decrease in lung peribronchial inflammatory score compared to WT mice (Fig. 3C). Additionally, RIPK3-deficient mice displayed a significant reduction in the number of macrophages and total cells in BAL fluid (Fig. 3D). Then, we asked whether RIPK3 would modulate AM necroptosis during RSV infection by examining the necrotic AM population in BAL samples of *Ripk3-/-* and WT mice. In fact, *Ripk3-/-* mice exhibited a significant decrease in the frequency of necrotic AM ($CD11c^+F4/80^+Siglec\text{-}F^+$fixable viability dye^+) in BAL fluid following RSV infection when compared to WT mice (Fig. 3E and Supplementary Fig. 4). These results indicate that RIPK3 exacerbates lung pathology during RSV infection *in vivo* and this is partially coupled to AM death outcomes.

Alveolar macrophages play a detrimental role during RSV infection in vivo.

The role played by AM during respiratory viral infections has been a matter of debate. AM seem to be essential for the early antiviral response against RSV infection [27, 28]. On the other hand, depletion of AM has been shown to be associated with a significant amelioration of disease, including attenuated weight loss without altering viral load during RSV reinfection of neonatally infected mice [29]. To establish the role of AM during RSV infection, we depleted these cells by an intranasal administration of clodronate-liposomes 24 h prior infection in mice. AM depletion was first confirmed by flow cytometry analysis of BAL cells, using anti-CD11c, anti-F4/80 and anti-Siglec-F antibodies recognizing mouse AM. A 3-fold significant reduction in AM numbers was observed in BAL of mice treated with clodronate-liposomes for 24 h compared to PBS-liposomes-treated mice (Supplementary Fig. 5A, B). After RSV infection, AM-depleted mice demonstrated significantly less weight loss (Fig. 4A) and a sharp reduction in lung viral loads when compared to non-depleted mice (Fig. 4B). Corresponding to the decrease in viral load, RSV F protein was not detected by immunohistochemical analysis of lung tissue of RSV-infected AM-depleted mice (Fig. 4C). Furthermore, AM depletion induced a significant decrease in lung histological inflammatory score in infected mice (Fig. 4D, E). As expected, AM-depleted mice displayed a lower number of macrophages in BAL, but surprisingly, a greater number of neutrophils (Fig. 4F). As a marker of cell damage, we measured LDH activity in BAL samples of mice. We were able to detect increased levels of LDH in BAL fluid of RSV-infected mice compared to uninfected ones; however, the treatment with clodronate-liposomes did not affect LDH release in mice (Fig. 4G). Interestingly, AM depletion abolished RIPK3 and MLKL mRNA upregulation in the lung tissue induced by RSV infection (Fig. 4H, I). Altogether, these data suggest that AM play a harmful role during RSV infection and that AM account for most of RIPK3 and MLKL expression in the lung tissue after infection.

Autocrine TNF mediates RSV-induced macrophage necroptosis *in vitro*.

We have recently shown that macrophages respond to *ex vivo* RSV infection by releasing TNF [30]. As TNF has been extensively studied as a necroptotic trigger [31], we sought to elucidate the role of TNF on RSV-induced macrophage necroptosis. RSV elicited the secretion of TNF by macrophages in a concentration-dependent manner (Fig. 5A), but only the replicating virus was able to induce TNF release (Fig. 5B). We next explored whether TNF would play a role on macrophage necroptosis triggered by RSV by treating the cells with a therapeutic TNF-specific neutralizing antibody (infliximab), a chimeric (mouse/human) antibody that cross-reacts with murine TNF [32]. Macrophages were treated with infliximab immediately before RSV infection. Neutralization of TNF with infliximab abolished macrophage necroptosis induced by RSV *in vitro* (Fig. 5C). Interestingly, blocking TNF secretion with brefeldin A, a well-known protein transport inhibitor [33], decreased TNF concentrations in macrophage supernatants to the control levels (mock) (Supplementary Fig. 6A) and profoundly reduced macrophage death caused by RSV (Supplementary Fig. 6B). We then infected macrophages from *Tnfr1-/-* and littermate control WT mice with RSV *ex vivo*. Notably, *Tnfr1-/-* macrophages were completely protected from RSV-induced death (Fig. 5D). Next, we sought to further elucidate the role of necroptosis pathways on TNF release induced by RSV infection. The pharmacological inhibition of RIPK1, RIPK3 and MLKL significantly reduced TNF secretion promoted by RSV in human monocytes (Fig. 5E), suggesting that necroptosis pathways are necessary for RSV-elicited TNF release. Lastly, we observed that the infection of human monocytes with two different RSV clinical isolates was able to induce TNF release (Fig. 5F). Collectively, these results indicate that RSV-triggered macrophage necroptosis is mediated by autocrine TNF and that necroptosis pathways are involved in TNF release.

Lack of TNFR1 signaling ameliorates RSV infection-induced pathology and diminishes AM necroptosis.

Based on our findings that autocrine TNF mediates RSV-induced macrophage necroptosis *ex vivo*, we were interested in elucidating the role of TNF on RSV infection and on RSV-induced AM necroptosis *in vivo*. Therefore, *Tnfr1-/-* and littermate WT mice were infected with RSV. Our results demonstrate that *Tnfr1-/-* mice were protected from RSV-induced body weight loss (Fig. 6A) and displayed significantly lower viral loads in the lung tissue (Fig. 6B) when compared to WT mice. Moreover, *Tnfr1-/-* mice presented a decrease in histological peribronchial and perivascular inflammation scores in comparison to WT mice (Fig.6C). The number of total leukocytes in BAL fluid of *Tnfr1-/-* mice was significantly lower after RSV infection, as well as the number of macrophages, when compared to WT mice (Fig. 6D). Interestingly, the expression of CXCL1 mRNA in the lung tissue of *Tnfr1-/-* mice was profoundly impaired (Fig. 6E), confirming that the inflammation was dampened

during RSV infection in these mice. Similarly, the expression of RIPK3 and MLKL transcripts was significantly reduced in *Tnfr1-/-* mice (Fig. 6F, G), suggesting that TNF mediates the expression of RIPK3 and MLKL in the lung tissue following RSV infection. Finally, we asked whether the lack of TNFR1 signaling would influence AM necroptosis during RSV infection by analyzing the necrotic AM population in BAL samples of *Tnfr1-/-* and WT mice. Remarkably, *Tnfr1-/-* mice displayed a 6-fold decrease in the frequency of necrotic AM ($CD11c^{+}F4/80^{+}$Siglec-F^{+}fixable viability dye^{+}) in BAL fluid following RSV infection when compared to WT mice (Fig. 6H and Supplementary Fig. 7). Altogether, these data strongly suggest that TNFR1 signaling mediates lung pathology and AM necroptosis triggered by RSV infection.

Elevated TNF levels in nasal wash correlate with disease severity in infants with RSV bronchiolitis.

We assessed the contribution of TNF during acute RSV infection by measuring TNF levels in nasal wash samples from infants with RSV bronchiolitis. There were no significant differences in age ($p = 0.6784$), sex ($p = 0.1507$) or birth weight ($p = 0.4484$) among patients from the RSV+ group compared to the RSV- group (Supplementary Table 1). The concentrations of TNF were significantly greater in the nasal samples from RSV+ infants (209.41 ± 23.55 pg/mL; n= 39) compared to RSV- infants (113.38 ± 14.16 pg/mL; n = 5), $p = 0.0014$ (Fig. 7A). We next analyzed the levels of TNF with respect to the need of supplemental oxygen therapy. There was a trend towards a positive correlation between the levels of TNF and the need for oxygen therapy measured in days, although it was not significant ($p = 0.0649$) (Fig. 7B). In contrast, there was a significant positive correlation between TNF levels in nasal wash and the length of hospital stay ($p = 0.0010$) (Fig. 7C). Interestingly, the infants who had a longer stay in the hospital (> 7 days) exhibited greater concentrations of TNF in the nasal wash (341.6 ± 60.24 pg/mL) compared to the ones who stayed less than 7 days in the hospital (119.7 ± 17.93 pg/mL), $p = 0.0002$ (Fig. 7D). These data suggest that elevated TNF levels in the nasal wash positively correlate with disease severity in infants with RSV infection.

Discussion

Respiratory viruses have been shown to trigger necroptosis in different cell types [16, 34-36]. Accordingly, recent studies have reported that RSV induces necroptosis in alveolar epithelial cells and THP-1 cells [19, 20]. However, whether RSV is able to trigger necroptosis in primary macrophages, important cells for the immune response against this viral infection, has not been investigated. In this study, we demonstrate that RSV infection induces alveolar and peritoneal mouse macrophage necroptosis in a concentration- and time-dependent manner. Moreover, RSV replicative activity was essential for necroptosis induction, since UV-inactivated RSV failed to trigger macrophage death. We extended our findings by showing that human monocytes, THP-1 cells and U937 cells differentiated to macrophage-like cells are all susceptible to RSV infection-triggered necroptosis. Importantly, in an effort to use a clinically representative strain of RSV, we infected human monocytes with two distinct RSV community isolates and we demonstrate that these isolates were able to promote necroptosis.

Necroptosis can occur when caspase-8 activity is compromised, and it is well known that virus-encoded caspase-8 inhibitors may switch the cell death program to necroptosis, as is the case for vaccinia virus (VV). VV-infected cells are susceptible to TNF-induced, RIPK1- and RIPK3-dependent necroptosis due to the expression of B13R, a caspase-8 inhibitor [15, 37, 38]. To date, there is no description in the literature of an RSV-encoded caspase-8 inhibitor. Thus, in an attempt to inhibit caspase-8 activity, we treated macrophages with the pancaspase inhibitor, zVAD-FMK, prior to RSV infection. However, in our setting, zVAD-FMK was unable to further increase macrophage necroptosis induced by RSV, indicating that RSV infection is sufficient to induce necroptosis. Our data is supported by previous findings showing that RSV naturally triggers alveolar epithelial cell necroptosis [20].

The interaction of RIPK1 and RIPK3 through the RIP homotypic interaction motif (RHIM)-RHIM domains is central to necroptotic signaling and leads to necrosome formation [39], which results in the mutual phosphorylation and activation of RIPK1 and RIPK3 [40]. The activation of RIPK3 causes the phosphorylation of its substrate, MLKL, which in turn oligomerizes and translocates to the plasma membrane, where it forms membrane-disrupting pores, leading to cell lysis [41-44]. Thus, to characterize the requirement of RIPK1 during RSV-elicited alveolar macrophage necroptosis, we treated the cells with NEC-1, which blocks the kinase activity of RIPK1 [25]. Indeed, treating macrophages with NEC-1 significantly decreased cell death induced by RSV. Furthermore, RIPK3 has shown to be essential for RSV-triggered necroptosis, since *Ripk3-/-* macrophages were completely resistant to cell death promoted by the virus and the pharmacological suppression of RIPK3

practically abolished human monocyte necroptosis caused by RSV infection. Likewise, NSA inhibition of MLKL profoundly impaired RSV-incited human monocyte necroptosis. Importantly, we found that RSV induced both RIPK3 and MLKL mRNA expression at 6 h post-infection. We also observed that the pharmacological inhibition or genetic deletion of necroptosis pathways markedly reduced viral loads in alveolar macrophages and human monocytes, suggesting that necroptosis promotes RSV persistence in these cells. Consistent with our findings, RIPK3 has been shown to facilitate coxsackievirus replication in intestinal epithelial cells [45]. Therefore, alveolar macrophages and human monocytes clearly rely on RIPK1, RIPK3 and MLKL to undergo cell death and these molecules act as positive regulators of RSV replication.

Based on the importance of RIPK3 for *in vitro* macrophage necroptosis triggered by RSV, we assumed that RIPK3 would be crucial for RSV-induced disease *in vivo*. In fact, the genetic deficiency of RIPK3 protected mice from RSV-induced weight loss and reduced the viral load in the lungs. Additionally, *Ripk3-/-* mice displayed an impaired recruitment of macrophages to the lungs, which may be secondary to the reduction of viral replication in the absence of RIPK3. Thus, we provide evidence for a detrimental role of RIPK3 during RSV infection. Similarly, RIPK3 deficiency protected mice from the infection with Influenza H7N9 virus by decreasing weight loss and the infiltration of inflammatory cells in the lungs [18]. Interestingly, it has been previously shown that RIPK3 simultaneously activates both MLKL-driven necroptosis and FADD-mediated apoptosis to protect against the spread of Influenza A H1N1 virus infection [16]. However, RIPK3 has been reported to promote inflammation and regulation of viral replication without triggering cell death [46]. In our setting, RIPK3 exacerbated lung injury by promoting inflammation and alveolar macrophage necroptosis, in some extent. Hence, the physiological relevance of RIPK3 during a viral infection may be determined by the virus subtype and likely interfering factors in the host immune response. As an important piece for necrosome formation, RIPK1 was also shown to be detrimental during viral bronchiolitis in mice, as both pharmacological blockade and genetic deficiency of RIPK1 protected mice from weight loss, neutrophilic inflammation and alarmin release [20]. Therefore, RIPK1 and RIPK3 are pathologic players during RSV infection.

The impact that AM have on respiratory virus-induced disease has been controversial. While AM seem to be essential for the early antiviral response against RSV infection [27, 28, 47, 48] and to prevent lethal Influenza pneumonia [49], the depletion of AM has been shown to be associated with a significant amelioration of disease, including attenuated weight loss and decreased airway obstruction, following pulmonary coronavirus and human metapneumovirus infection in mice [27, 50]. Moreover, AM depletion prolonged survival in response to acute pneumovirus infection in mice

and reduced weight loss without altering viral load during RSV reinfection of neonatally infected mice [29, 51]. Our data clearly demonstrate that AM enhance RSV replication in the lungs and significantly contribute to clinical disease and lung pathology. These findings were consistently underlined by the reduction in lung viral loads, attenuated weight loss and impaired peribronchial inflammation score in AM-depleted mice. Thus, it is reasonable to assume that AM may represent the first immune cell target of RSV infection in the lungs, acting as virus factories in the early phase of disease. Importantly, AM depletion abolished the upregulation of RIPK3 and MLKL mRNA induced by RSV infection, suggesting that AM account for most of RIPK3 and MLKL expression in the lung tissue after infection, prompting them to undergo necroptosis.

As macrophage necroptosis triggered by RSV required virus replication, we hypothesized that during RSV replication cycle, the necroptotic machinery was activated indirectly, for example, through the autocrine activity of a virus-induced pro-necroptotic cytokine, such as TNF. Consistent with this assumption, we have recently shown that macrophages respond to RSV infection by secreting TNF [30]. We extended these findings and show that RSV triggers the release of TNF in a concentration-dependent manner and that TNF is released as a result of RSV replication, as UV-inactivated RSV is not able to induce TNF secretion from macrophages. Then, we were interested in investigating whether TNF would mediate RSV-promoted macrophage necroptosis. The neutralization of TNF with infliximab, a therapeutic anti-TNF antibody, abolished macrophage necroptosis induced by RSV. Interestingly, when TNF secretion was blocked by brefeldin A, RSV effect over macrophage death was lost. Moreover, Tnfr1-deficient macrophages were completely resistant to RSV-triggered cell death. Thus, our findings establish that TNF is secreted during RSV replication in alveolar macrophages, which in turn, in an autocrine manner, promotes macrophage necroptosis. Furthermore, it has been recently shown that RIPK3 activation leads to cytokine production even after loss of plasma membrane integrity [52]. Hence, we decided to clarify whether RIPK1, RIPK3 and MLKL would promote TNF synthesis in the context of RSV-induced necroptosis. Indeed, the pharmacological blockade of necroptosis proteins markedly impaired TNF secretion triggered by RSV infection. These data imply that besides inducing TNF production through its replicative activity in macrophages, RSV also leads to TNF synthesis through activation of the necroptotic machinery even when macrophages are committed to cell death. The secretion of TNF by necroptosis activation could lead to a positive feedback loop, worsening lung pathology induced by RSV infection. In line with our findings, influenza virus, which also elicits RIPK3-mediated necroptosis [16, 35], has been reported to promote such phenomenon [52].

Given our observation on the participation of TNF during *in vitro* RSV infection of alveolar macrophages, we sought to elucidate the role of TNF on RSV infection and on RSV-induced AM necroptosis *in vivo*. In our setting, the lack of TNFR1 signaling has shown to be protective against RSV-induced weight loss and lung inflammation. In addition, *Tnfr1-/-* mice presented a sharp reduction in viral loads and in the infiltration of macrophages in the lungs. In accordance, mice lacking both TNF and IL-1 receptors exhibited decreased lung inflammation and a significant delay in mortality caused by a lethal challenge with H5N1 virus [53]. Furthermore, TNF and macrophages have been shown to be critical to RSV-induced asthma exacerbations in mice [54]. Notably, we found that the expression of *Ripk3* and *Mlkl* genes was significantly impaired in the lungs of *Tnfr1-/-* mice following RSV infection, which may reflect the profound reduction in the percent of necrotic AM in the absence of TNFR1 signaling. We provide compelling evidence that TNF is critically involved in the severity of clinical disease during RSV infection by increasing viral load and lung pathology, as well as promoting RIPK3- and MLKL-dependent AM necroptosis. In support of our findings, it has been previously demonstrated that TNF-induced necroptosis requires the activation of RIPK1, RIPK3 and MLKL in different cell types and in mouse models [41, 55, 56]. In addition, RIPK1-RIPK3-mediated cellular damage by necroptosis drives mortality during TNF-induced systemic inflammatory response syndrome (SIRS) [57].

Previous studies have shown that TNF, together with other pro-inflammatory cytokines, is elevated in the nasal wash of infants infected with RSV [58-60]. Corroborating with the previous findings, our results demonstrate that RSV-infected infants exhibit higher levels of TNF in the nasal wash compared to infants infected with other respiratory viruses. TNF signaling within the respiratory tract governs different pathophysiological functions of the airways, including inflammatory cell recruitment and activation to pathogens [61]. A possible mechanism by which high levels of TNF may increase disease severity is through the upregulation of adhesion molecules on small capillaries, thereby inducing the recruitment of inflammatory cells into the airways, such as neutrophils, macrophages and eosinophils [62]. Also, TNF has been recently reported to be involved in bronchoconstriction during RSV infection in mice [63]. We measured disease severity in infants on the basis of the length of hospital stay and the duration of supplemental oxygen therapy. We were not able to find a positive correlation between the levels of TNF and the need for oxygen therapy; however, we did find a significant positive association between TNF levels in nasal wash and the length of hospital stay. Interestingly, we found that the infants who stayed more than 7 days in the hospital presented greater concentrations of TNF in the nasal wash compared to the ones who stayed less than 7 days in the hospital. Collectively, these data suggest that elevated TNF levels in the nasal wash positively correlates with disease severity in infants with RSV infection. Moreover, it

has been previously shown that RSV bronchiolitis is associated with TNF haplotypes [64], suggesting that the genetically mediated upregulation of TNF might support an exaggerated inflammation in the airways and thus promote a more severe course of RSV infection.

In conclusion, our data demonstrate that autocrine TNF mediates RIPK1-, RIPK3-, MLKL-dependent alveolar macrophage necroptosis triggered by RSV infection and that necroptosis pathways are detrimental to viral clearance. Moreover, TNF-mediated alveolar macrophage necroptosis plays an important role in the pathogenesis of RSV infection (Fig. 8). Additionally, we provide evidence that elevated nasal levels of TNF are associated with disease severity in infants with RSV bronchiolitis. We propose that targeting TNF and/or the necroptotic machinery may be valuable as an additional therapeutic approach to reduce the respiratory morbidity caused by RSV infection in young children and babies.

Acknowledgments.

We thank Géssica Antunes, Deise do Nascimento de Freitas, Rodrigo Dornelles, Janaína Pasetti Nunes (all from PUCRS) and Rosemeire Florença de Paula (UNICAMP) for their excellent technical assistance. We also thank the Rheumatology Service of São Lucas Hospital (Porto Alegre, Rio Grande do Sul, Brazil) for kindly donating Infliximab (Remicade; Centocor).

Support Statement.

This study was supported by Conselho Nacional de Desenvolvimento Científico e Tecnológico (CNPq) grant nr. 456282/2014-9 (to BNP) and Coordenação de Aperfeiçoamento de Pessoal de Nível Superior (CAPES) – Finance Code 001.

References

1. Meissner HC. Viral Bronchiolitis in Children. N Engl J Med. 2016;374(18):1793-4.
2. Nair H, Nokes DJ, Gessner BD, et al. Global burden of acute lower respiratory infections due to respiratory syncytial virus in young children: a systematic review and meta-analysis. Lancet. 2010;375(9725):1545-55.
3. Geoghegan S, Erviti A, Caballero MT, et al. Mortality due to Respiratory Syncytial Virus. Burden and Risk Factors. Am J Respir Crit Care Med. 2017;195(1):96-103.
4. Langley GF, Anderson LJ. Epidemiology and prevention of respiratory syncytial virus infections among infants and young children. Pediatr Infect Dis J. 2011;30(6):510-7.
5. Blanken MO, Rovers MM, Molenaar JM, et al. Respiratory syncytial virus and recurrent wheeze in healthy preterm infants. N Engl J Med. 2013;368(19):1791-9.
6. Mohapatra SS, Boyapalle S. Epidemiologic, experimental, and clinical links between respiratory syncytial virus infection and asthma. Clin Microbiol Rev. 2008;21(3):495-504.
7. Hussell T, Bell TJ. Alveolar macrophages: plasticity in a tissue-specific context. Nat Rev Immunol. 2014;14(2):81-93.
8. Martin WJ, 2nd, Wu M, Pasula R. A novel approach to restore lung immunity during systemic immunosuppression. Trans Am Clin Climatol Assoc. 2005;116:221-6; discussion 6-7.
9. Gordon S, Pluddemann A, Martinez Estrada F. Macrophage heterogeneity in tissues: phenotypic diversity and functions. Immunol Rev. 2014;262(1):36-55.
10. Downey J, Pernet E, Coulombe F, et al. Dissecting host cell death programs in the pathogenesis of influenza. Microbes Infect. 2018;20(9-10):560-9.
11. Fan R, Wen B, Liu W, et al. Altered regulatory cytokine profiles in cases of pediatric respiratory syncytial virus infection. Cytokine. 2018;103:57-62.
12. Weinlich R, Oberst A, Beere HM, et al. Necroptosis in development, inflammation and disease. Nat Rev Mol Cell Biol. 2017;18(2):127-36.
13. Hitomi J, Christofferson DE, Ng A, et al. Identification of a molecular signaling network that regulates a cellular necrotic cell death pathway. Cell. 2008;135(7):1311-23.
14. Sun L, Wang H, Wang Z, et al. Mixed lineage kinase domain-like protein mediates necrosis signaling downstream of RIP3 kinase. Cell. 2012;148(1-2):213-27.
15. Cho YS, Challa S, Moquin D, et al. Phosphorylation-driven assembly of the RIP1-RIP3 complex regulates programmed necrosis and virus-induced inflammation. Cell. 2009;137(6):1112-23.
16. Nogusa S, Thapa RJ, Dillon CP, et al. RIPK3 Activates Parallel Pathways of MLKL-Driven Necroptosis and FADD-Mediated Apoptosis to Protect against Influenza A Virus. Cell Host Microbe. 2016;20(1):13-24.
17. Rodrigue-Gervais IG, Labbe K, Dagenais M, et al. Cellular inhibitor of apoptosis protein cIAP2 protects against pulmonary tissue necrosis during influenza virus infection to promote host survival. Cell Host Microbe. 2014;15(1):23-35.
18. Xu YL, Tang HL, Peng HR, et al. RIP3 deficiency ameliorates inflammatory response in mice infected with influenza H7N9 virus infection. Oncotarget. 2017;8(17):27715-24.
19. Bedient L, Pokharel SM, Chiok KR, et al. Lytic Cell Death Mechanisms in Human Respiratory Syncytial Virus-Infected Macrophages: Roles of Pyroptosis and Necroptosis. Viruses. 2020;12(9).
20. Simpson J, Loh Z, Ullah MA, et al. Respiratory Syncytial Virus Infection Promotes Necroptosis and HMGB1 Release by Airway Epithelial Cells. Am J Respir Crit Care Med. 2020;201(11):1358-71.

21. Villani A, Cirino NM, Baldi E, et al. Respiratory syncytial virus infection of human mononuclear phagocytes stimulates synthesis of platelet-activating factor. J Biol Chem. 1991;266(9):5472-9.
22. Newton K, Sun X, Dixit VM. Kinase RIP3 is dispensable for normal NF-kappa Bs, signaling by the B-cell and T-cell receptors, tumor necrosis factor receptor 1, and Toll-like receptors 2 and 4. Mol Cell Biol. 2004;24(4):1464-9.
23. Barends M, de Rond LG, Dormans J, et al. Respiratory syncytial virus, pneumonia virus of mice, and influenza A virus differently affect respiratory allergy in mice. Clin Exp Allergy. 2004;34(3):488-96.
24. Galluzzi L, Kroemer G. Necroptosis: a specialized pathway of programmed necrosis. Cell. 2008;135(7):1161-3.
25. Degterev A, Hitomi J, Germscheid M, et al. Identification of RIP1 kinase as a specific cellular target of necrostatins. Nat Chem Biol. 2008;4(5):313-21.
26. Yan B, Liu L, Huang S, et al. Discovery of a new class of highly potent necroptosis inhibitors targeting the mixed lineage kinase domain-like protein. Chem Commun (Camb). 2017;53(26):3637-40.
27. Kolli D, Gupta MR, Sbrana E, et al. Alveolar macrophages contribute to the pathogenesis of human metapneumovirus infection while protecting against respiratory syncytial virus infection. Am J Respir Cell Mol Biol. 2014;51(4):502-15.
28. Pribul PK, Harker J, Wang B, et al. Alveolar macrophages are a major determinant of early responses to viral lung infection but do not influence subsequent disease development. J Virol. 2008;82(9):4441-8.
29. Harker JA, Yamaguchi Y, Culley FJ, et al. Delayed sequelae of neonatal respiratory syncytial virus infection are dependent on cells of the innate immune system. J Virol. 2014;88(1):604-11.
30. de Souza GF, Muraro SP, Santos LD, et al. Macrophage migration inhibitory factor (MIF) controls cytokine release during respiratory syncytial virus infection in macrophages. Inflamm Res. 2019;68(6):481-91.
31. Wajant H, Siegmund D. TNFR1 and TNFR2 in the Control of the Life and Death Balance of Macrophages. Front Cell Dev Biol. 2019;7:91.
32. Seadi Pereira PJ, Noronha Dornelles F, Santiago Santos D, et al. Nociceptive and inflammatory responses induced by formalin in the orofacial region of rats: effect of anti-TNFalpha strategies. Int Immunopharmacol. 2009;9(1):80-5.
33. Fujiwara T, Oda K, Yokota S, et al. Brefeldin A causes disassembly of the Golgi complex and accumulation of secretory proteins in the endoplasmic reticulum. J Biol Chem. 1988;263(34):18545-52.
34. Gaba A, Xu F, Lu Y, et al. The NS1 Protein of Influenza A Virus Participates in Necroptosis by Interacting with MLKL and Increasing Its Oligomerization and Membrane Translocation. J Virol. 2019;93(2).
35. Thapa RJ, Ingram JP, Ragan KB, et al. DAI Senses Influenza A Virus Genomic RNA and Activates RIPK3-Dependent Cell Death. Cell Host Microbe. 2016;20(5):674-81.
36. Meessen-Pinard M, Le Coupanec A, Desforges M, et al. Pivotal Role of Receptor-Interacting Protein Kinase 1 and Mixed Lineage Kinase Domain-Like in Neuronal Cell Death Induced by the Human Neuroinvasive Coronavirus OC43. J Virol. 2017;91(1).
37. Chan FK, Shisler J, Bixby JG, et al. A role for tumor necrosis factor receptor-2 and receptor-interacting protein in programmed necrosis and antiviral responses. J Biol Chem. 2003;278(51):51613-21.
38. Li M, Beg AA. Induction of necrotic-like cell death by tumor necrosis factor alpha and caspase inhibitors: novel mechanism for killing virus-infected cells. J Virol. 2000;74(16):7470-7.

39. Li J, McQuade T, Siemer AB, et al. The RIP1/RIP3 necrosome forms a functional amyloid signaling complex required for programmed necrosis. Cell. 2012;150(2):339-50.
40. Vandenabeele P, Declercq W, Van Herreweghe F, et al. The role of the kinases RIP1 and RIP3 in TNF-induced necrosis. Sci Signal. 2010;3(115):re4.
41. Cai Z, Jitkaew S, Zhao J, et al. Plasma membrane translocation of trimerized MLKL protein is required for TNF-induced necroptosis. Nat Cell Biol. 2014;16(1):55-65.
42. Dondelinger Y, Declercq W, Montessuit S, et al. MLKL compromises plasma membrane integrity by binding to phosphatidylinositol phosphates. Cell Rep. 2014;7(4):971-81.
43. Hildebrand JM, Tanzer MC, Lucet IS, et al. Activation of the pseudokinase MLKL unleashes the four-helix bundle domain to induce membrane localization and necroptotic cell death. Proc Natl Acad Sci U S A. 2014;111(42):15072-7.
44. Wang H, Sun L, Su L, et al. Mixed lineage kinase domain-like protein MLKL causes necrotic membrane disruption upon phosphorylation by RIP3. Mol Cell. 2014;54(1):133-46.
45. Harris KG, Morosky SA, Drummond CG, et al. RIP3 Regulates Autophagy and Promotes Coxsackievirus B3 Infection of Intestinal Epithelial Cells. Cell Host Microbe. 2015;18(2):221-32.
46. Daniels BP, Snyder AG, Olsen TM, et al. RIPK3 Restricts Viral Pathogenesis via Cell Death-Independent Neuroinflammation. Cell. 2017;169(2):301-13 e11.
47. Goritzka M, Makris S, Kausar F, et al. Alveolar macrophage-derived type I interferons orchestrate innate immunity to RSV through recruitment of antiviral monocytes. J Exp Med. 2015;212(5):699-714.
48. Reed JL, Brewah YA, Delaney T, et al. Macrophage impairment underlies airway occlusion in primary respiratory syncytial virus bronchiolitis. J Infect Dis. 2008;198(12):1783-93.
49. Cardani A, Boulton A, Kim TS, et al. Alveolar Macrophages Prevent Lethal Influenza Pneumonia By Inhibiting Infection Of Type-1 Alveolar Epithelial Cells. PLoS Pathog. 2017;13(1):e1006140.
50. Hartwig SM, Holman KM, Varga SM. Depletion of alveolar macrophages ameliorates virus-induced disease following a pulmonary coronavirus infection. PloS one. 2014;9(3):e90720.
51. Rigaux P, Killoran KE, Qiu Z, et al. Depletion of alveolar macrophages prolongs survival in response to acute pneumovirus infection. Virology. 2012;422(2):338-45.
52. Orozco SL, Daniels BP, Yatim N, et al. RIPK3 Activation Leads to Cytokine Synthesis that Continues after Loss of Cell Membrane Integrity. Cell Rep. 2019;28(9):2275-87 e5.
53. Perrone LA, Szretter KJ, Katz JM, et al. Mice lacking both TNF and IL-1 receptors exhibit reduced lung inflammation and delay in onset of death following infection with a highly virulent H5N1 virus. J Infect Dis. 2010;202(8):1161-70.
54. Nguyen TH, Maltby S, Simpson JL, et al. TNF-alpha and Macrophages Are Critical for Respiratory Syncytial Virus-Induced Exacerbations in a Mouse Model of Allergic Airways Disease. J Immunol. 2016;196(9):3547-58.
55. Polykratis A, Hermance N, Zelic M, et al. Cutting edge: RIPK1 Kinase inactive mice are viable and protected from TNF-induced necroptosis in vivo. J Immunol. 2014;193(4):1539-43.
56. Remijsen Q, Goossens V, Grootjans S, et al. Depletion of RIPK3 or MLKL blocks TNF-driven necroptosis and switches towards a delayed RIPK1 kinase-dependent apoptosis. Cell Death Dis. 2014;5:e1004.
57. Duprez L, Takahashi N, Van Hauwermeiren F, et al. RIP kinase-dependent necrosis drives lethal systemic inflammatory response syndrome. Immunity. 2011;35(6):908-18.

58. Bennett BL, Garofalo RP, Cron SG, et al. Immunopathogenesis of respiratory syncytial virus bronchiolitis. J Infect Dis. 2007;195(10):1532-40.
59. Laham FR, Israele V, Casellas JM, et al. Differential production of inflammatory cytokines in primary infection with human metapneumovirus and with other common respiratory viruses of infancy. J Infect Dis. 2004;189(11):2047-56.
60. McNamara PS, Flanagan BF, Selby AM, et al. Pro- and anti-inflammatory responses in respiratory syncytial virus bronchiolitis. Eur Respir J. 2004;23(1):106-12.
61. Mukhopadhyay S, Hoidal JR, Mukherjee TK. Role of TNFalpha in pulmonary pathophysiology. Respir Res. 2006;7:125.
62. Lukacs NW, Strieter RM, Chensue SW, et al. TNF-alpha mediates recruitment of neutrophils and eosinophils during airway inflammation. J immunol. 1995;154(10):5411-7.
63. Morris DR, Ansar M, Ivanciuc T, et al. Selective Blockade of TNFR1 Improves Clinical Disease and Bronchoconstriction in Experimental RSV Infection. Viruses. 2020;12(10).
64. Puthothu B, Bierbaum S, Kopp MV, et al. Association of TNF-alpha with severe respiratory syncytial virus infection and bronchial asthma. Pediatric Allergy and Immunology. 2009;20(2):157-63.

Figure Legends

Fig. 1. RSV induces necrosis in primary mouse macrophages, human monocytes and macrophage-like cell lines. (A) Balb/c mice-derived alveolar macrophages ($3x10^5$/well) were infected with RSV (MOI 1) or with UV-RSV (MOI 1) for 6 h at 37°C under 5% CO_2. Then, cells were labeled with Fixable Viability Dye eFluor® 780, harvested and the percent of dead cells was analyzed by flow cytometry. **(B)** Alveolar macrophages ($3x10^5$/well) were infected with RSV (MOI 1) or left uninfected for 6 h at 37°C with 5% CO_2. Afterwards, RNA was harvested and RSV viral load was quantified the by real-time PCR and expressed as copies/mL. **(C)** Balb/c mice-derived peritoneal macrophages ($3x10^5$/well) were infected with RSV (MOI 1) or with UV-RSV (MOI 1) for 6 h. Then, cells were harvested and labeled with Fixable Viability Dye eFluor® 780 and the percent of dead cells was analyzed by flow cytometry. **(D)** Human monocytes ($3x10^5$/well) were infected with two distinct community isolates of RSV (MOI 1) for 6 h. Afterwards, cells were labeled with Fixable Viability Dye eFluor® 780, harvested and the percent of dead cells was analyzed by flow cytometry. Data are representative of 3 independent experiments performed in triplicates and represent mean ± SEM. Data were analyzed with one-way ANOVA (A, C and D) or unpaired Student's *t* test (B). *$p < 0.05$; **$p < 0.01$; ***$p < 0.001$; ****$p < 0.0001$. ND = not detected.

Fig. 2. RIPK1, RIPK3 and MLKL are required for RSV-induced macrophage necroptosis. (A and B) Balb/c mice-derived macrophages ($3x10^5$/well) were treated with zVAD-FMK (Sigma-Aldrich, Saint Louis, MO, USA) (20 μM) (A) or with NEC-1 (Sigma-Aldrich, Saint Louis, MO, USA) (30 μM) (B) for 1 h prior to RSV infection (MOI 1) for 6 h. Afterwards, macrophages were labeled with Fixable Viability Dye eFluor® 780, harvested and the percent of dead cells was analyzed by flow cytometry. **(C)** Alveolar macrophages ($3x10^5$/well) from *Ripk3*-/- and littermate control WT mice were infected *ex vivo* with RSV (MOI 1) for 6 h. Afterwards, cell death was assessed by LDH release in macrophages supernatants and expressed as % LDH release. **(D and E)** Human monocytes ($3x10^5$/well) were treated with GW42X (Synkinase, Parkville, VIC, Australia) (2 μM) (D) or with NSA (Millipore, Billerica, MA, USA) (2 μM) (E) for 1 h prior to RSV infection (MOI 1) for 6 h. Then, cells were labeled with Fixable Viability Dye eFluor® 780, harvested and the percent of dead cells was analyzed by flow cytometry. **(F)** Macrophages were treated with zVAD-FMK (20 μM), NEC-1 (30 μM), GW42X (2 μM) or with NSA (2 μM) for 1 h prior to RSV infection (MOI 1) for 6 h. Afterwards, RNA was harvested and RSV viral load was quantified the by real-time PCR and expressed as copies/mL. **(G)** Macrophages ($3x10^5$/well) from *Ripk3*-/- and littermate control WT mice were infected *ex vivo* with RSV (MOI 1) for 6 h. Then, RNA was harvested and RSV viral load was quantified the by real-time PCR and expressed as copies/mL. **(H and I)** Alveolar macrophages were infected with RSV (MOI 1) for 2, 4 or 6 h.

Afterwards, RNA was harvested and *Ripk3* mRNA (H) and *Mlkl* mRNA (I) expression was quantified by real-time PCR using $2^{-\Delta Ct}$ method and expressed as fold change. Data are representative of at least 2 independent experiments performed in triplicates and represent mean ± SEM. Data were analyzed with one-way ANOVA with Tukey's post-hoc test (A, B, C, D, E, F, H and I) or unpaired Student's *t* test (G). *$p < 0.05$; **$p < 0.01$; ***$p < 0.001$; ****$p < 0.0001$. ns = not significant; ND = not detected.

Fig. 3. RIPK3 exacerbates lung pathology during RSV infection partially dependent on cell death. *Ripk3*-/- and littermate control WT mice were infected with RSV (10^7 PFU/animal). Data analysis was performed 5 days post infection. **(A)** Percent of body weight loss post infection relative to initial weight (day 0) (n = 5). **(B)** RSV viral load detected in the lung tissue by real-time PCR (viral copies/g lung) (n = 3). **(C)** Representative images of lung tissue sections stained with hematoxylin-eosin and its respective inflammation scores (n = 3). Scale bars = 200 μm. **(D)** Total cell number and differential cell counting in BAL fluid (n = 3). **(E)** Percent of necrotic alveolar macrophages ($CD11c^+F4/80^+Siglec\text{-}F^+$fixable viability dye^+) in BAL fluid and its representative FACS profile (n = 4 – 5). Data are representative of 2 independent experiments and are expressed as mean ± SEM. Data were analyzed with one-way ANOVA with Bonferroni's post-hoc test (A) or with Mann-Whitney test (B, C, D and E). *$p < 0.05$; **$p < 0.01$; ***$p < 0.001$.

Fig. 4. Alveolar macrophages play a detrimental role during RSV infection in vivo. Balb/c mice were depleted of alveolar macrophages by an intranasal administration of clodronate-liposomes (500μg/animal) or PBS-liposomes. Mice were infected with RSV (10^7 PFU/animal) 24 hours later. Data analysis was performed 5 days post infection. **(A)** Percent of body weight loss post infection relative to initial weight (day 0) (n = 5). **(B)** RSV viral load detected in the lung tissue by real-time PCR (viral copies/g lung) (n = 4 – 5). **(C)** Representative images of immunohistochemical staining of lung tissues using an anti-RSV Fusion protein antibody. Scale bars = 200 μm. **(D)** Representative images of lung tissue sections stained with hematoxylin-eosin. Scale bars = 200 μm. **(E)** Peribronchial and perivascular inflammation scores respective to histological images shown in D (n = 3). **(F)** Total cell number and differential cell counting in BAL fluid (n = 4 – 5). **(G)** Lactate dehydrogenase (LDH) activity (OD 490 nm) in BAL samples (n = 4 – 5). **(H and I)** *Ripk3* mRNA (H) and *Mlkl* mRNA (I) expression in the lung tissue quantified by real-time PCR using $2^{-\Delta Ct}$ method and expressed as fold change (n = 3 – 4). Data are representative of 2 independent experiments and are expressed as mean ± SEM. Data were analyzed with one-way ANOVA with Tukey's post-hoc test. *$p < 0.05$; **$p < 0.01$; ***$p < 0.001$. UI = uninfected; ND = not detected.

Fig. 5. Autocrine TNF mediates RSV-induced macrophage necroptosis *in vitro*. (A and B) Balb/c mice-derived macrophages ($3x10^5$/well) were infected with increasing MOIs of RSV (0.1 – 5) for 6 h

(A) or with active or UV-inactivated RSV (MOI 1) for 6 h (B). Afterwards, the supernatants were collected and TNF concentrations were measured by ELISA. **(C)** Balb/c mice-derived macrophages ($3x10^5$/well) were infected with RSV (MOI 1) in the presence of infliximab (10 μg/mL) for 6 h. Then, cells were labeled with Fixable Viability Dye eFluor® 780, harvested and the percent of dead cells was analyzed by flow cytometry. **(D)** Alveolar macrophages ($3x10^5$/well) from *Tnfr1*-/- and littermate control WT mice were infected *ex vivo* with RSV (MOI 1) for 6 h. Afterwards, cell death was assessed by LDH release in macrophages supernatants. **(E)** Human monocytes ($3x10^5$/well) were treated with NEC-1 (30 μM), GW42X (2 μM) or with NSA (2 μM) for 1 h prior to RSV infection (MOI 1) for 6 h. Then, cell supernatants were collected and TNF concentrations were measured by ELISA. **(F)** Human monocytes ($3x10^5$/well) were infected with two distinct community isolates of RSV (MOI 1) for 6 h. Afterwards, cell supernatants were collected and TNF concentrations were measured by ELISA. Data are representative of at least 2 independent experiments performed in triplicates and represent mean ± SEM. Data were analyzed with one-way ANOVA with Tukey's post-hoc test. ***$p < 0.001$; ****$p < 0.0001$.

Fig. 6. Lack of TNFR1 signaling ameliorates RSV infection-induced pathology and diminishes AM necroptosis. *Tnfr1*-/- and littermate control WT mice were infected with RSV (10^7 PFU/animal). Data analysis was performed 5 days post infection. **(A)** Percent of body weight loss post infection relative to initial weight (day 0) (n = 5). **(B)** RSV viral load detected in the lung tissue by real-time PCR (viral copies/g lung) (n = 4). **(C)** Representative images of lung tissue sections stained with hematoxylin-eosin and its respective inflammation scores (n = 3). Scale bars = 200 μm. **(D)** Total cell number and differential cell counting in BAL fluid (n = 3). **(E, F and G).** *Cxcl1* mRNA (E), *Ripk3* mRNA (F) and *Mlkl* mRNA (G) expression in the lung tissue quantified by real-time PCR using $2^{-\Delta Ct}$ method (n = 3). **(H)** Percent of necrotic alveolar macrophages ($CD11c^+F4/80^+Siglec\text{-}F^+$fixable viability dye^+) in BAL fluid and its representative FACS profile (n = 4). Data are representative of 2 independent experiments and are expressed as mean ± SEM. Data were analyzed with unpaired Student's *t* test. *$p < 0.05$; **$p < 0.01$; ***$p < 0.001$.

Fig.7. Elevated TNF levels in nasal wash correlate with disease severity in infants with RSV bronchiolitis. Nasal wash samples were collected from infants up to 12 months of age who were admitted to the hospital with acute bronchiolitis. The presence of RSV was confirmed by real-time PCR. **(A)** TNF levels were measured by ELISA in the supernatants of nasal wash and compared among infants positive for RSV and infants negative for RSV. **(B)** Spearman linear correlation between TNF levels (pg/mL) and time of O_2 need (days) of infants with acute bronchiolitis (RSV+). **(C)** Spearman linear correlation between TNF levels (pg/mL) and hospital length (days) of infants with acute

bronchiolitis (RSV+). **(D)** Comparison of TNF levels among RSV+ infants who spent $<$ 7 days at hospital and who spent $>$ 7 days at hospital. Data are expressed as mean $\pm$ SEM and were analyzed with unpaired Student's *t* test (A and D). **p = 0.0014; ***p = 0.0002.

Fig. 8. Mechanisms of RSV-induced macrophage necroptosis. During RSV infection in macrophages, TNF is produced and secreted as a result of viral replication and activation of the necroptotic machinery. In an autocrine manner, TNF binds to TNFR1, leading to RIPK1 and RIPK3 phosphorylation. As a consequence of RIPK3 activation, MLKL is phosphorylated and activated, leading to macrophage necroptosis. In mice, RSV-induced TNF-mediated alveolar macrophage necroptosis results in weight loss, increased lung viral loads and exacerbated lung inflammation.

Fig. S1. (A and B) Balb/c mice-derived alveolar macrophages ($3x10^5$/well) were infected with different MOIs of RSV (0.1 – 10) for 6 h at 37°C with 5% CO_2. Afterwards, cells were harvested and labeled with Fixable Viability Dye eFluor® 780 and the percent of dead cells was analyzed by flow cytometry (A) or cell death was assessed by LDH release in macrophages supernatants and expressed as % LDH release (B). **(C)** Alveolar macrophages ($3x10^5$/well) were infected with RSV (MOI 1) for 2, 4 or 6 h. Afterwards, cells were harvested and labeled with Fixable Viability Dye eFluor® 780 and the percent of dead cells was analyzed by flow cytometry. **(D)** Balb/c mice-derived peritoneal macrophages ($3x10^5$/well) were infected with different MOIs of RSV (0.1 – 10) for 6 h at 37°C with 5% CO_2. Afterwards, cells were harvested and labeled with Fixable Viability Dye eFluor® 780 and the percent of dead cells was analyzed by flow cytometry. **(E)** Balb/c mice-derived peritoneal macrophages ($3x10^5$/well) were infected with different MOIs of RSV (0.1 – 10) for 6 h. Then, cell death was assessed by LDH release in macrophages supernatants and expressed as % LDH release. **(F)** Peritoneal macrophages ($3x10^5$/well) were infected with RSV (MOI 1) for 2, 4 or 6 h. After that, cell death was assessed by LDH release in macrophages supernatants and expressed as % LDH release. Data are representative of 3 independent experiments performed in triplicates and represent mean $\pm$ SEM. Data were analyzed with one-way ANOVA with Tukey's post-hoc test. *p $<$ 0.05; ***p $<$ 0.001; ****p $<$ 0.0001.

Fig. S2. (A, D) Human monocytes ($3x10^5$/well) were infected with RSV (MOI 1) for 6 h. Afterwards, cells were harvested and labeled with Fixable Viability Dye eFluor® 780 and the percent of dead cells was analyzed by flow cytometry (A) or cell death was assessed by LDH release in cell supernatants and expressed as % LDH release (D). **(B, E)** THP-1 cells ($2x10^5/cm^2$) were infected with RSV (MOI 1) for 6 h. After that, cells were harvested and labeled with Fixable Viability Dye eFluor® 780 and the percent of dead cells was analyzed by flow cytometry (B) or cell death was assessed by LDH release in cell supernatants and expressed as % LDH release (E). **(C, F)** U937 cells ($2x10^5/cm^2$)

were differentiated to macrophage-like cells with PMA (50 ng/mL) for 24 h. After differentiation, cells were infected with RSV (MOI 1) for 6 h. Then, cells were harvested and labeled with Fixable Viability Dye eFluor® 780 and the percent of dead cells was analyzed by flow cytometry (C) or cell death was assessed by LDH release in cell supernatants and expressed as % LDH release (F). **(G)** A549 cells, human monocytes, THP-1 cells and U937 cells ($3x10^5$/well) were infected with RSV (MOI 1) for 6 h. Then, RNA was harvested and RSV viral loads were quantified the by real-time PCR and expressed as copies/mL. Data are representative of 3 independent experiments performed in triplicates and represent mean ± SEM. Data were analyzed with unpaired Student's *t* test. **$p < 0.01$; ***$p < 0.001$; ****$p < 0.0001$.

Fig. S3. Balb/c mice-derived alveolar macrophages were infected with RSV (MOI 1) for 2, 4 or 6 h. Cell lysates were examined for MLKL expression by western blot. The densitometry analysis was performed using ImageJ 1.43 software (NIH). MLKL bands were normalized to GAPDH bands. Data are representative of 2 independent experiments with similar results.

Fig. S4. Gating strategy used in the flow cytometry analysis of necrotic alveolar macrophages obtained from WT and *Ripk3*-/- mice infected with RSV. **(A)** BAL cells were collected from infected WT and *Ripk3*-/- mice and stained for CD11c, F4/80, Siglec-F and fixable viability dye. Single cells 1 were gated based on FSC-H x FSC-A plot. Single cells 2 were gated based on SSC-W x SSC-A plot inside single cells 1. $CD11c^+F4/80^+$ population was gated inside single cells 2. Siglec-F^+ population was gated inside $CD11c^+F4/80^+$ gate. Fixable viability dye^+ population (necrotic cells) was gated inside Siglec-F^+ gate. **(B)** Representative FACS profile of necrotic WT and *Ripk3*-/- alveolar macrophages ($CD11c^+F4/80^+$Siglec-F^+fixable viability dye^+) after RSV infection.

Fig. S5. Gating strategy used in the flow cytometry analysis of alveolar macrophage numbers in BAL fluid of mice treated with clodronate-liposomes or PBS-liposomes for 24 h (n = 4). **(A)** BAL cells were collected from mice treated with clodronate-liposomes or PBS-liposomes and stained for CD11c, F4/80 and Siglec-F. Single cells 1 were gated based on FSC-H x FSC-A plot. Single cells 2 were gated based on SSC-W x SSC-A plot inside single cells 1. $CD11c^+$ population was gated inside single cells 2. $F4/80^+$Siglec-F^+ population was obtained inside $CD11c^+$ gate. **(B)** Representative FACS profile and absolute numbers of alveolar macrophages ($CD11c^+F4/80^+$Siglec-F^+) in BAL fluid of clodronate-liposomes or PBS-liposomes-treated mice. Data were analyzed with unpaired Student's *t* test. **$p < 0.01$.

Fig. S6. (A) Balb/c mice-derived macrophages ($3x10^5$/well) were infected with RSV (MOI 1) for 6 h alone or in the presence of brefeldin A (BD GolgiStop™, BD Bioscience, San Jose, CA, USA) (0.5

μg/mL) added in the last 4 h. Afterwards, the supernatants were collected and TNF concentrations were measured by ELISA. **(B)** Macrophages ($3x10^5$/well) were infected with RSV (MOI 1) for 6 h alone or in the presence of brefeldin A added in the last 4 h. Then, macrophages were harvested and labeled with Fixable Viability Dye eFluor® 780 and the percent of dead cells was analyzed by flow cytometry. Data are representative of 2 independent experiments performed in triplicates and represent mean ± SEM. Data were analyzed with one-way ANOVA with Tukey's post-hoc test. **$p < 0.01$; ****$p < 0.0001$.

Fig. S7. Gating strategy used in the flow cytometry analysis of necrotic alveolar macrophages obtained from WT and *Tnfr1*-/- mice infected with RSV. **(A)** BAL cells were collected from infected WT and *Tnfr1*-/- mice and stained for CD11c, F4/80, Siglec-F and fixable viability dye. Single cells 1 were gated based on FSC-H x FSC-A plot. Single cells 2 were gated based on SSC-W x SSC-A plot inside single cells 1. $CD11c^+F4/80^+$ population was gated inside single cells 2. Siglec-F^+ population was gated inside $CD11c^+F4/80^+$ gate. Fixable viability dye^+ population (necrotic cells) was gated inside Siglec-F^+ gate. **(B)** Representative FACS profile of necrotic WT and *Tnfr1*-/- alveolar macrophages ($CD11c^+F4/80^+$Siglec-F^+fixable viability dye^+) after RSV infection.

Table S1. Characteristics of the study population

	RSV positive (n = 39)	RSV negative (n = 5)	95% CI	*P* value
Age (months)	3.434 ± 1.787	3.807 ± 2.665	-2.171 to 1.426	0.6784
Sex (M/F)	28/11	2/3		0.1507*
Birth weight (kg)	3.084 ± 848.5	3.336 ± 590.9	-420.9 to 925.8	0.4484

Values are presented as the mean ± standard deviation for age and birth weight (unpaired *t* test analysis). RSV, respiratory syncytial virus; CI, confidence interval; M, male; F, female. * *P* value for chi-square test.

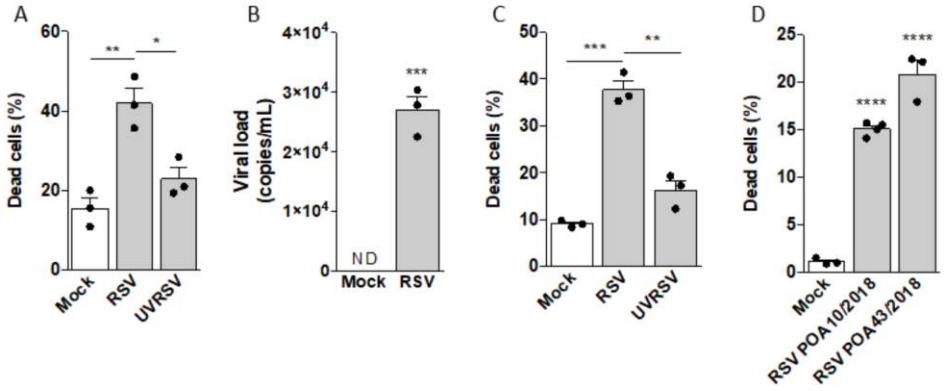
A
Dead cells (%)
60
40
20
0
**
*
Mock
RSV
UVRSV
B
Viral load (copies/mL)
4×10^4
3×10^4
2×10^4
1×10^4
0
***
ND
Mock
RSV
C
Dead cells (%)
50
40
30
20
10
0
***
**
Mock
RSV
UVRSV
D
Dead cells (%)
25
20
15
10
5
0
****
****
Mock
RSV POA10/2018
RSV POA43/2018

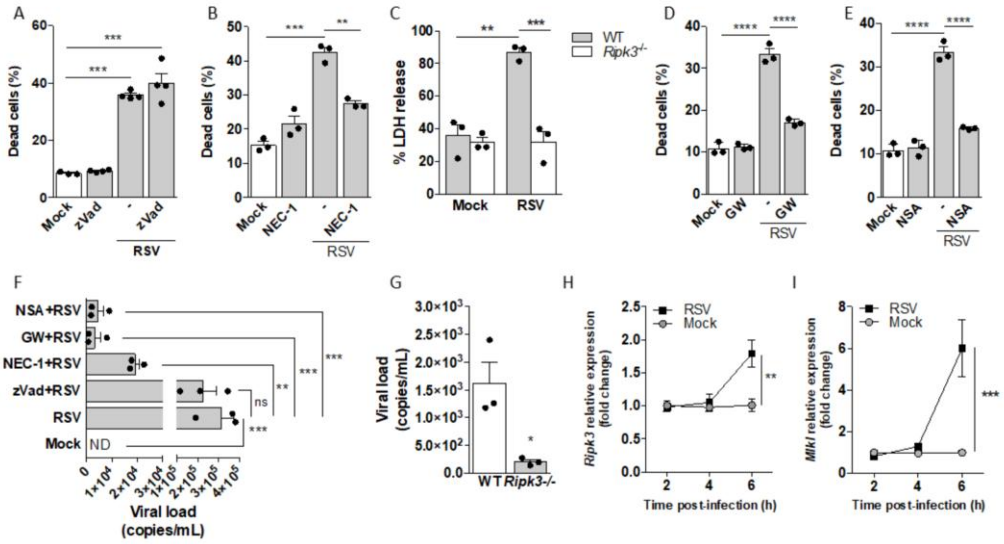
A
Dead cells (%)
Mock
zVad
-
zVad
RSV
B
Dead cells (%)
Mock
NEC-1
-
NEC-1
RSV
C
% LDH release
WT
Ripk3-/-
Mock
RSV
D
Dead cells (%)
Mock
GW
-
GW
RSV
E
Dead cells (%)
Mock
NSA
-
NSA
RSV
F
NSA+RSV
GW+RSV
NEC-1+RSV
zVad+RSV
RSV
Mock
ND
ns
Viral load (copies/mL)
G
Viral load (copies/mL)
WT
Ripk3-/-
H
Ripk3 relative expression (fold change)
RSV
Mock
Time post-infection (h)
I
Mlkl relative expression (fold change)
RSV
Mock
Time post-infection (h)

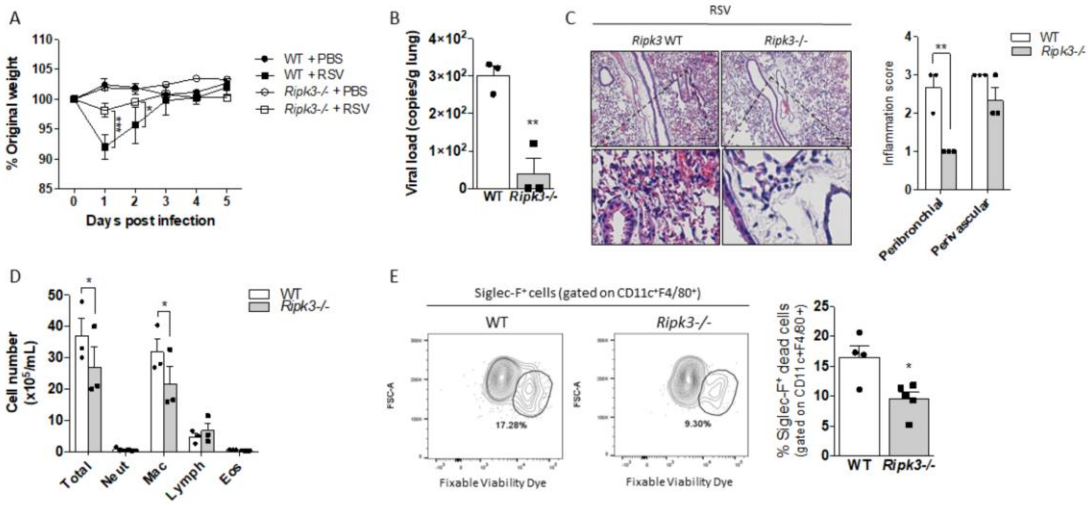
A
% Original weight
Days post infection
WT + PBS
WT + RSV
Ripk3-/- + PBS
Ripk3-/- + RSV
B
Viral load (copies/g lung)
WT
Ripk3-/-
C
RSV
Ripk3 WT
Ripk3-/-
Inflammation score
Peribronchial
Perivascular
WT
Ripk3-/-
D
Cell number (x10⁶/mL)
Total
Neut
Mac
Lymph
Eos
E
Siglec-F⁺ cells (gated on CD11c⁺F4/80⁺)
17.28%
9.30%
Fixable Viability Dye
% Siglec-F⁺ dead cells (gated on CD11c+F480+)

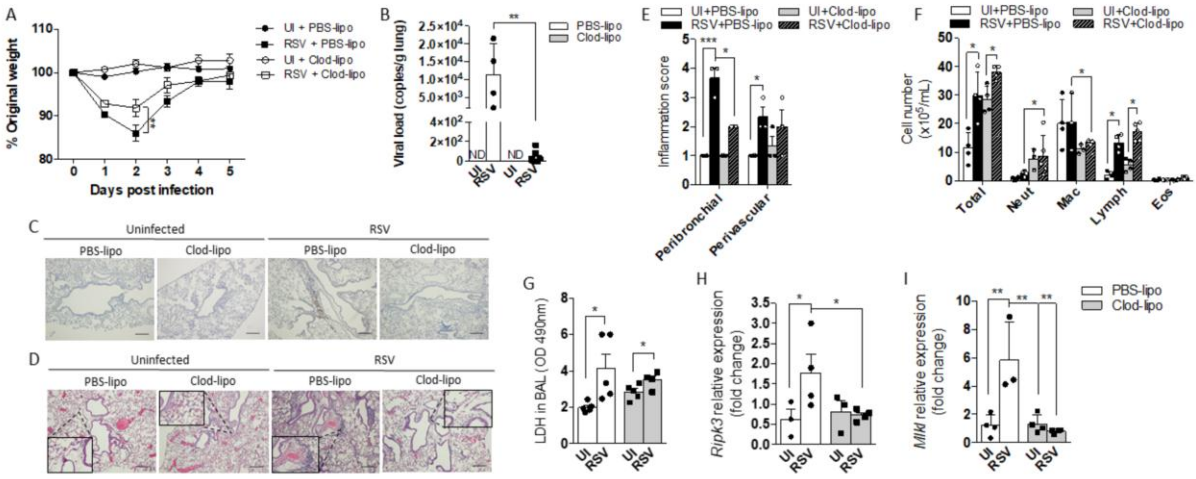
A
% Original weight
Days post infection
UI + PBS-lipo
RSV + PBS-lipo
UI + Clod-lipo
RSV + Clod-lipo
B
Viral load (copies/g lung)
PBS-lipo
Clod-lipo
ND
UI
RSV
C
Uninfected
RSV
PBS-lipo
Clod-lipo
D
E
Inflammation score
UI+PBS-lipo
RSV+PBS-lipo
UI+Clod-lipo
RSV+Clod-lipo
Peribronchial
Perivascular
F
Cell number (x10^5/mL)
Total
Neut
Mac
Lymph
Eos
G
LDH in BAL (OD 490nm)
H
Ripk3 relative expression (fold change)
I
Mlkl relative expression (fold change)

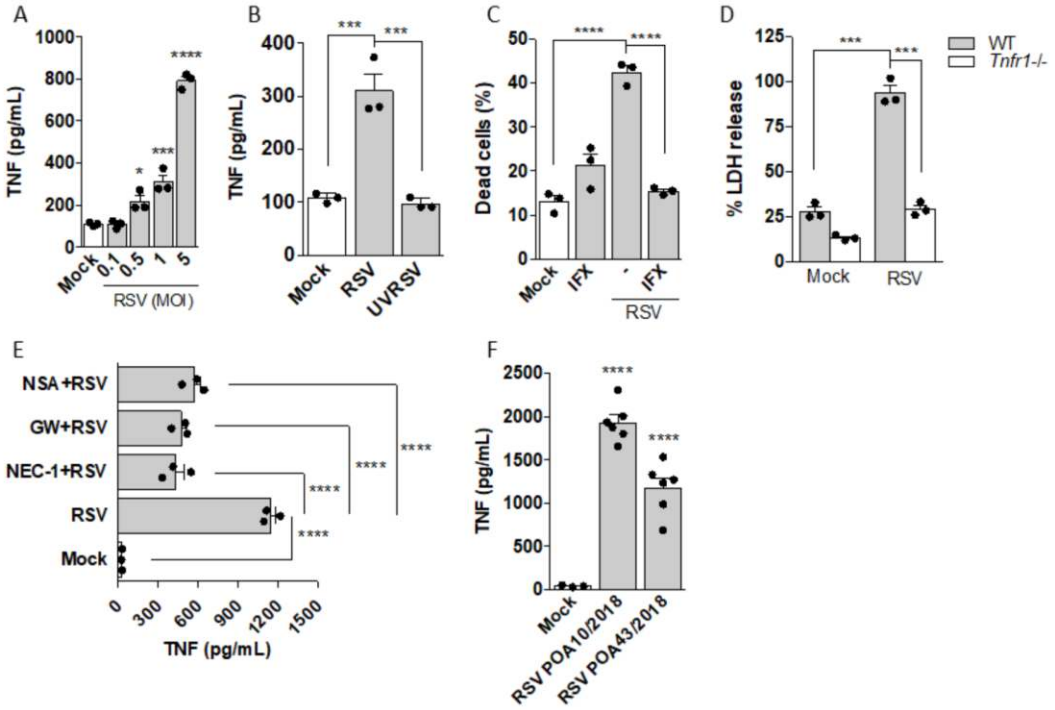
A
TNF (pg/mL)
Mock
0.1
0.5
1
5
RSV (MOI)
B
TNF (pg/mL)
Mock
RSV
UVRSV
C
Dead cells (%)
Mock
IFX
-
IFX
RSV
D
% LDH release
WT
Tnfr1-/-
Mock
RSV
E
NSA+RSV
GW+RSV
NEC-1+RSV
RSV
Mock
TNF (pg/mL)
F
TNF (pg/mL)
Mock
RSV POA10/2018
RSV POA43/2018

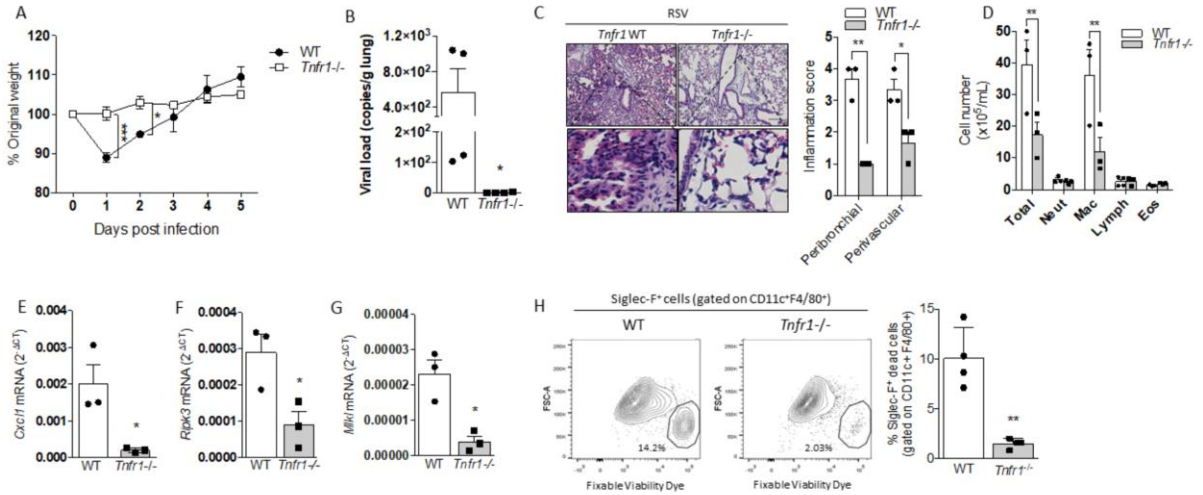
A
% Original weight
Days post infection
WT
Tnfr1-/-
B
Viral load (copies/g lung)
C
RSV
Tnfr1 WT
Tnfr1-/-
Inflammation score
Peribronchial
Perivascular
D
Cell number (x10^5/mL)
Total
Neut
Mac
Lymph
Eos
E
Cxcl1 mRNA (2^-ΔCT)
F
Rpk3 mRNA (2^-ΔCT)
G
Mlkl mRNA (2^-ΔCT)
H
Siglec-F+ cells (gated on CD11c+F4/80+)
14.2%
2.03%
Fixable Viability Dye
% Siglec-F+ dead cells (gated on CD11c+ F4/80+)

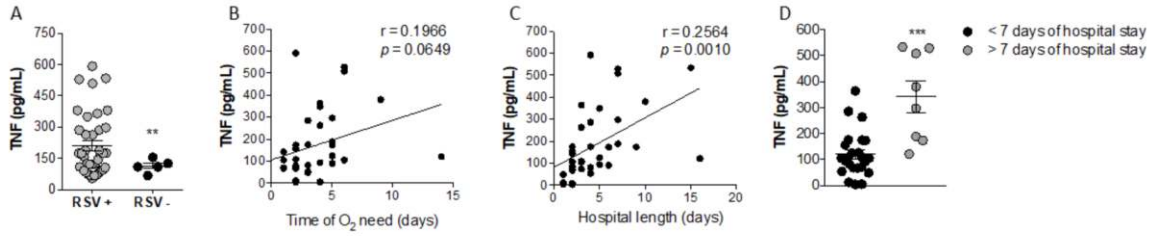
A
TNF (pg/mL)
750
600
450
300
150
0
**
RSV +
RSV -
B
TNF (pg/mL)
r = 0.1966
p = 0.0649
Time of O2 need (days)
C
TNF (pg/mL)
r = 0.2564
p = 0.0010
Hospital length (days)
D
TNF (pg/mL)
***
< 7 days of hospital stay
> 7 days of hospital stay

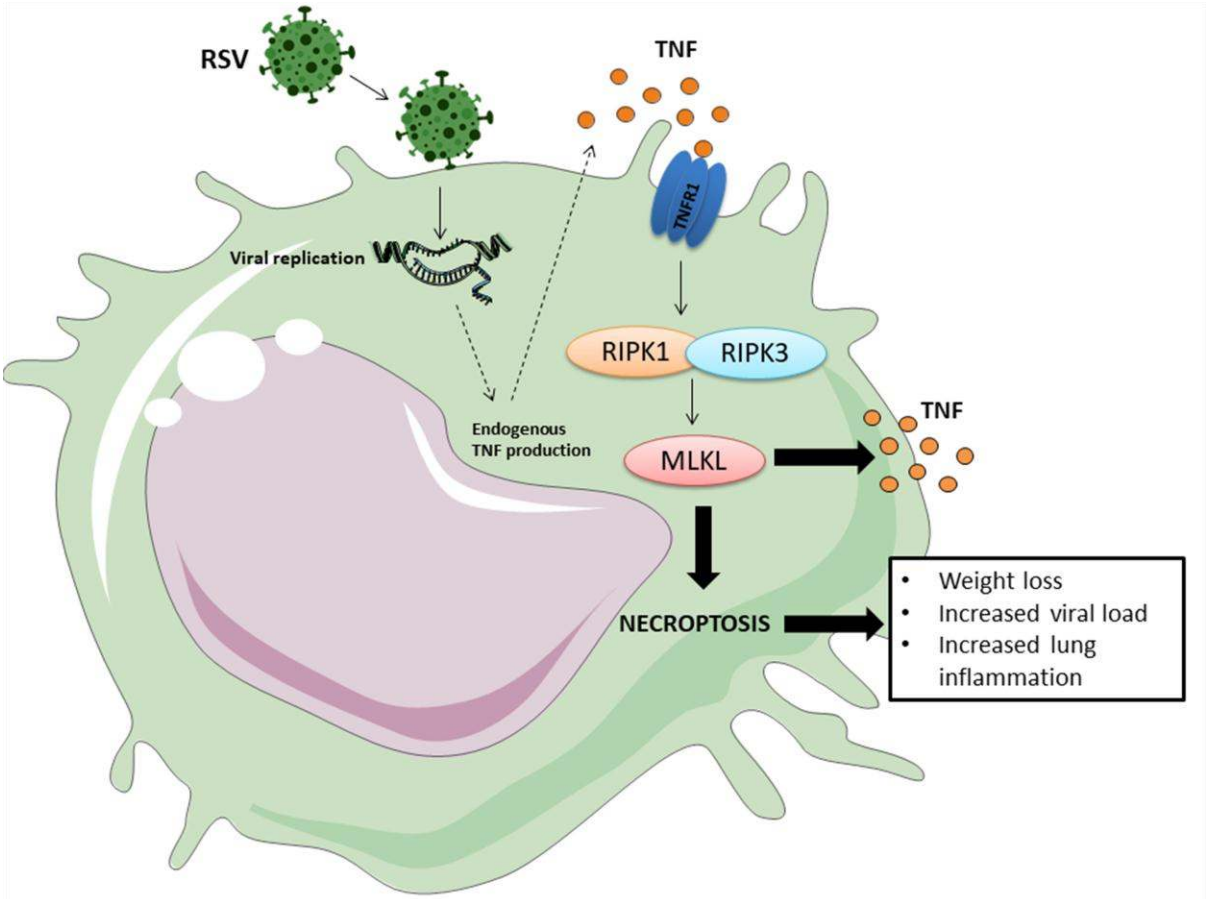
RSV
TNF
TNFR1
Viral replication
RIPK1
RIPK3
Endogenous
TNF production
MLKL
TNF
NECROPTOSIS
• Weight loss
• Increased viral load
• Increased lung inflammation

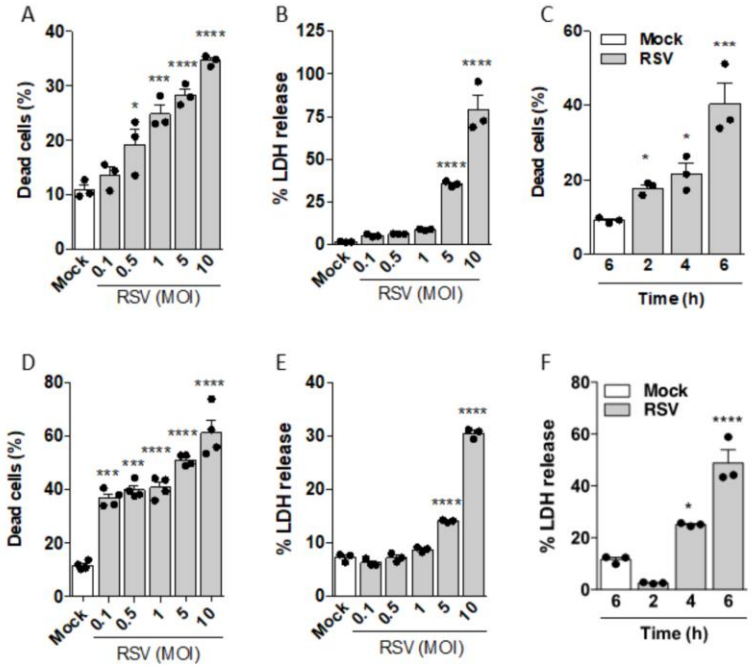
A
Dead cells (%)
Mock
0.1
0.5
1
5
10
RSV (MOI)
B
% LDH release
C
Mock
RSV
Time (h)
D
E
F

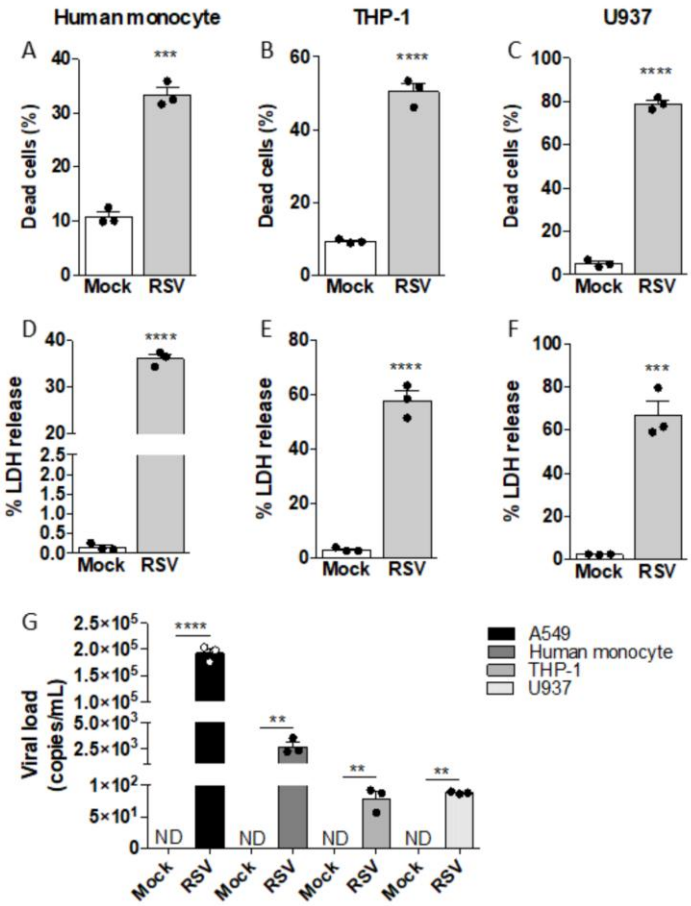
Human monocyte
THP-1
U937
A
B
C
D
E
F
G
Dead cells (%)
% LDH release
Viral load (copies/mL)
Mock
RSV
ND
A549
Human monocyte
THP-1
U937

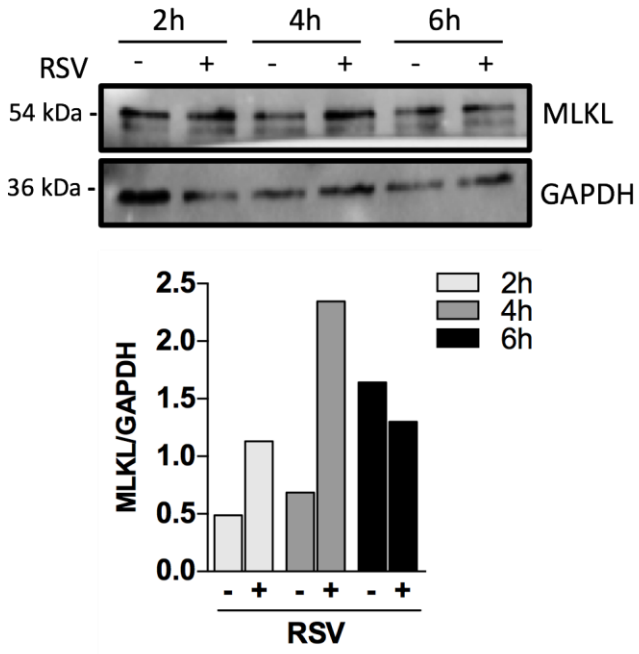
2h
4h
6h
RSV
- + - + - +
54 kDa
MLKL
36 kDa
GAPDH
MLKL/GAPDH
2.5
2.0
1.5
1.0
0.5
0.0
2h
4h
6h
- + - + - +
RSV

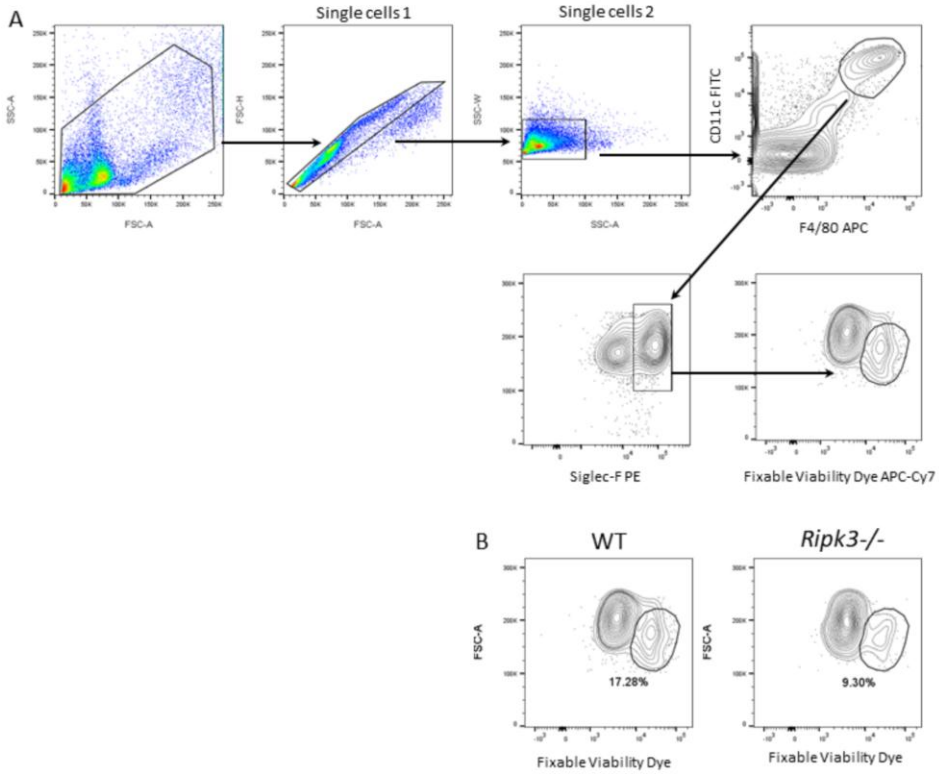
A
Single cells 1
Single cells 2
SSC-A
FSC-A
FSC-H
FSC-A
SSC-W
SSC-A
CD11c FITC
F4/80 APC
Siglec-F PE
Fixable Viability Dye APC-Cy7
B
WT
Ripk3-/-
FSC-A
17.28%
Fixable Viability Dye
FSC-A
9.30%
Fixable Viability Dye

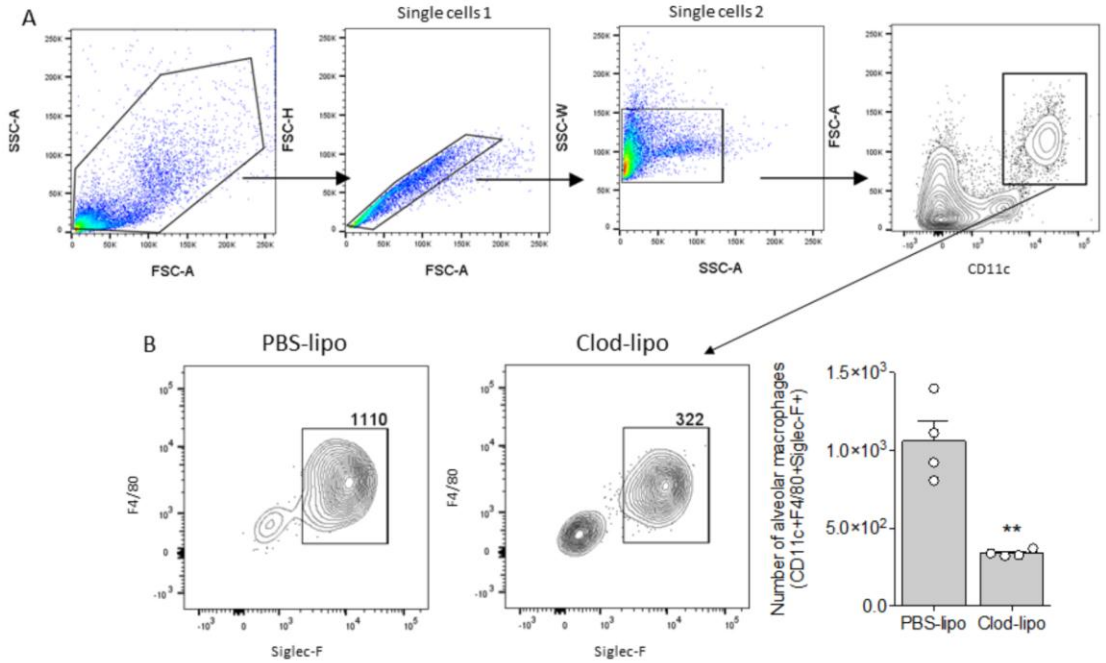
A
Single cells 1
Single cells 2
SSC-A
FSC-A
FSC-H
FSC-A
SSC-W
SSC-A
FSC-A
CD11c
B
PBS-lipo
Clod-lipo
1110
322
F4/80
Siglec-F
F4/80
Siglec-F
Number of alveolar macrophages (CD11c+F4/80+Siglec-F+)
1.5×10^3
1.0×10^3
5.0×10^2
0.0
**
PBS-lipo
Clod-lipo

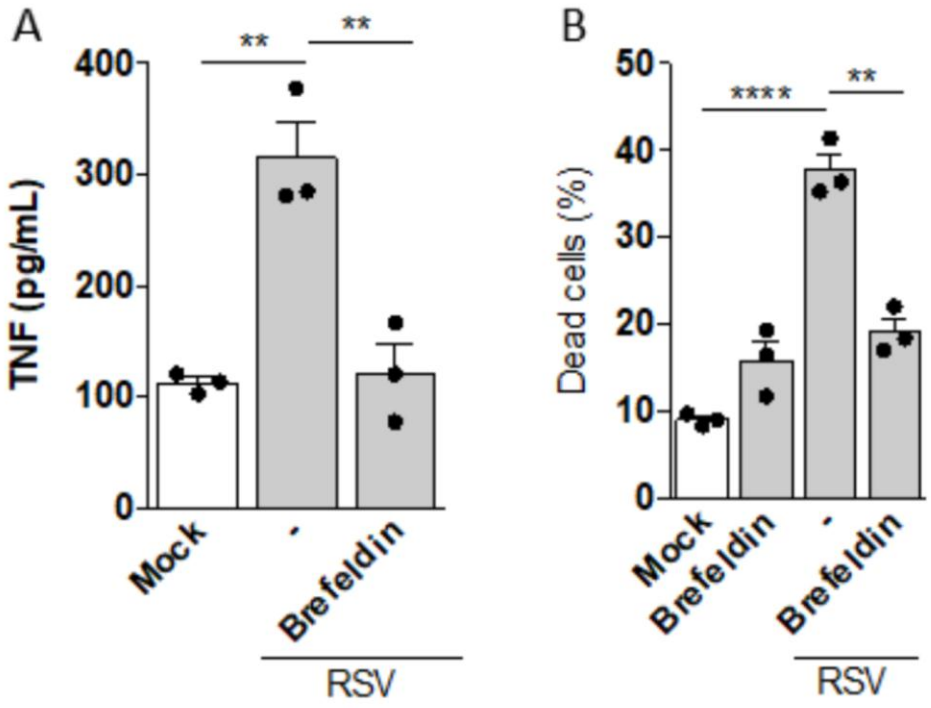
A
**
**
400
300
200
100
0
TNF (pg/mL)
Mock
-
Brefeldin
RSV
B
****
**
50
40
30
20
10
0
Dead cells (%)
Mock
Brefeldin
-
Brefeldin
RSV

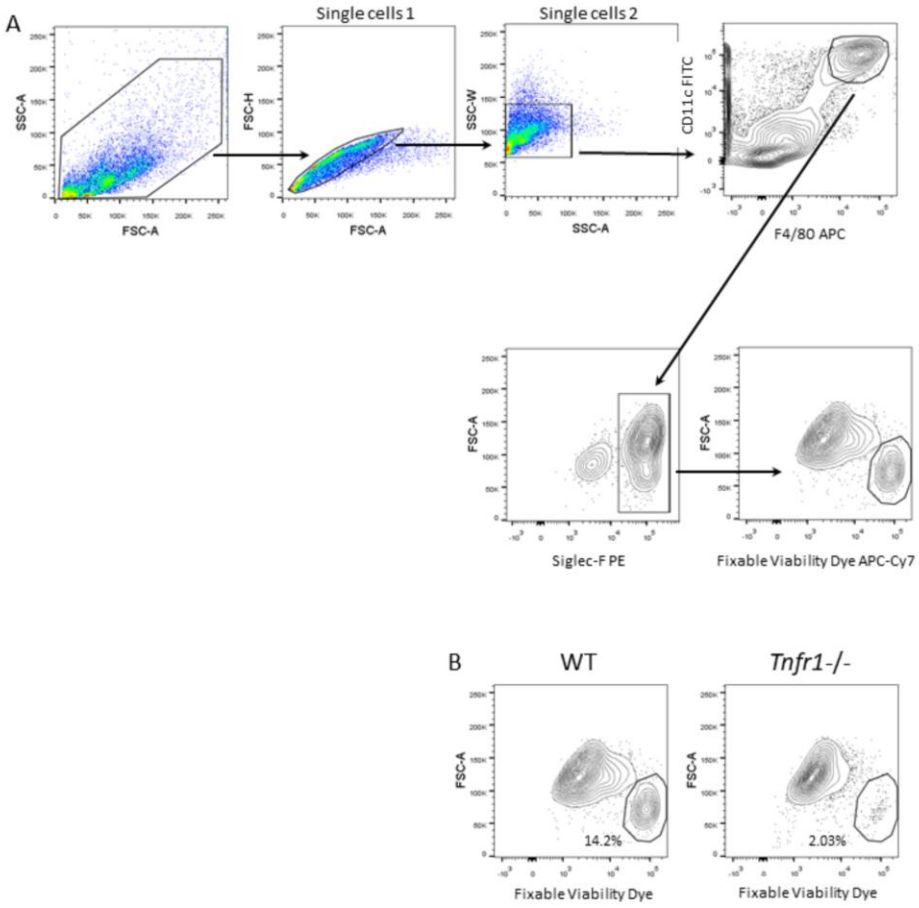
A
Single cells 1
Single cells 2
SSC-A
FSC-A
FSC-H
FSC-A
SSC-W
SSC-A
CD11c FITC
F4/80 APC
FSC-A
Siglec-F PE
FSC-A
Fixable Viability Dye APC-Cy7

B
WT
Tnfr1-/-
FSC-A
14.2%
Fixable Viability Dye
FSC-A
2.03%
Fixable Viability Dye